

CONTINUOUS DATA ASSIMILATION FOR TWO-PHASE FLOW: ANALYSIS AND SIMULATIONS

YAT TIN CHOW, WING TAT LEUNG, AND ALI PAKZAD

ABSTRACT. We propose, analyze, and test a novel continuous data assimilation two-phase flow algorithm for reservoir simulation. We show that the solutions of the algorithm, constructed using coarse mesh observations, converge at an exponential rate in time to the corresponding exact reference solution of the two-phase model. More precisely, we obtain a stability estimate which illustrates an exponential decay of the residual error between the reference and approximate solution, until the error hits a threshold depending on the order of data resolution. Numerical computations are included to demonstrate the effectiveness of this approach, as well as variants with data on sub-domains. In particular, we demonstrate numerically that synchronization is achieved for data collected from a small fraction of the domain.

1. INTRODUCTION

1.1. Data assimilation. Data assimilation (DA) refers to a class of methodologies which combines information from grain coarse observational data with simulation/dynamical model in order to obtain a more accurate forecast. The method has a long history, with applications in weather modeling and environmental forecasting [63], as well as the medical, environmental and biological science, [56, 58], imaging, traffic control, finance and oil exploration [6]. There are a variety of data assimilation techniques, with which actual measured quantities over time are incorporated in system models. One classical technique, which is based on a linear-quadratic estimation, is known as the Kalman filter. This Bayesian approach gives exact probabilistic predictions, although the underlying system and any corresponding observation models are assumed to be linear. This approach has been modified to cover more general cases in ensemble Kalman filter, extended Kalman filter and the unscented Kalman filter; see [8, 31, 60].

A major difficulty of applying a physical model to real life applications is that, usually the initial condition cannot be known/measured exactly, and only an approximation over a coarse spatial resolution is known. This imprecision in measuring the initial condition may sometimes cause an exponential growing error in the solution of a nonlinear system. To overcome this difficulty, a promising approach, known as the continuous data assimilation, was proposed and analyzed by Azouani, Olson, and Titi in [10, 11] based on techniques coming from control theory. This approach introduces a feedback control term at the PDE level to synchronize the computed solution with the true solution corresponding to the observed data.

Date: June 22, 2022.

2010 Mathematics Subject Classification. Primary: 76T05, 65M12, 76D55; Secondary: 35Q35, 35Q93.

Key words and phrases. Data assimilation, Multiphase flow.

To describe the method, we consider a dynamical system

$$(1.1) \quad \frac{d\mathbf{u}}{dt} = \mathbf{F}(\mathbf{u}),$$

with insufficient/inaccurate knowledge of the initial state $\mathbf{u}(0)$, but with a solution $\mathbf{u}(t)$ on a coarse grid that is believed to accurately reflect some aspects of the underlying physical reality. Given observational data of the system at a coarse spatial resolution of size H , i.e. $\Pi_H(\mathbf{u}(t))$ from some given interpolation operator Π_H , the algorithm is to construct an approximate solution $\mathbf{v}(t)$ from the observations that satisfies the auxiliary equation

$$(1.2) \quad \frac{d\mathbf{v}}{dt} = \mathbf{F}(\mathbf{v}) - \mu \Pi_H(\mathbf{v} - \mathbf{u}), \quad \mathbf{v}(0) = \text{arbitrary},$$

where $\mu > 0$ is a relaxation (nudging) parameter. The goal is to pick $\mu > 0$ and $H > 0$ such that

$$\mathbf{v}(t) \rightarrow \mathbf{u}(t)$$

as $t \rightarrow \infty$ in a suitable spatial space. The above algorithm is designed to work for many nonlinear dissipative dynamical systems of the form (1.1), with their solutions well-known to be unstable. Owing to this instability, it is expected that any small error in the initial data could lead to an exponentially growing error in the solutions. In these cases, the dissipative term (only) controls the small scales and instabilities occur at large scales. The feedback term in (1.2) that is newly introduced then aims to stabilize the system and damp the error term at large scales by forcing (nudging) the large spatial scales of the measured solution (of the auxiliary equation) back to the reference solution.

In the context of the incompressible 2D Navier-Stokes equations, the authors in [10] proved that, for large enough μ and small enough H , the approximate solution \mathbf{v} to (1.2), converges exponentially fast to the exact solution \mathbf{u} . Numerical experiments were carried out successfully to test this algorithm for many nonlinear systems, for instance, the 2D Navier-Stokes equation [17, 43, 44, 50, 59], the Rayleigh-Bénard equations [7, 33], and the Kuramoto-Sivashinsky equations [61]. Continuous data assimilation applied to other physical phenomena and PDEs includes non-Newtonian fluids [21], magnetohydrodynamic equations [15], Leray- α model of turbulence [52], quasi-geostrophic equation [52], Darcy's equation [64], KdV equations [51], primitive equations [70], and many others. While the aforementioned works assume noise-free observations, the method is later extended to the case when only noisy data can be obtained, e.g. in [12, 41, 49]. The authors refer the readers to other recent literature on this topic; see, e.g. [9, 16, 32, 34, 36–41, 46, 48, 61, 62, 68, 76].

1.2. Multi-phase flow. Thanks to the development of numerical reservoir simulation, oil-field corporations have deeply benefited from the technology in terms of confidently predicting oil recovery estimates and determining the selection of operations during the deployment of specific recovery technologies. During the screening stage, numerical reservoir model is established and simulations are run to determine the feasibility of many injection/production options. This requires reservoir simulation to be accurate and time efficient. Furthermore, for oil and gas reservoirs that are already in production, it is necessary to determine reservoir parameters (e.g. permeability, porosity) with increasing certainty [1, 65]. As the oil field matures, more effective practices such as production enhancement, chemical treatment or

infill drilling can greatly extend the life of the oil reservoir, thereby increasing the overall recovery rate.

A commonly used model in reservoir simulation is the multi-phase flow model [18, 57, 72, 74]. In recent decades, both the mathematical analysis and numerical simulation of the two-phase flows have been a focus of study for many researchers and practitioners, thanks to their important applications in petroleum engineering and hydrology. The system of equations governing two-phase immiscible incompressible flows in porous media consists of a nonlinear elliptic Darcy-type equation for the global pressure and a nonlinear parabolic equation with degenerate diffusion term for the saturation, which are coupled by means of the total velocity, recuperated from Darcy's equation [4, 23, 26].

Due to the nonlinear nature of the problem, the velocity of the fluid in different phases highly depends on the saturation and the pressure of the respective phase. So as to obtain an accurate simulation, we are required to have a good initialization of the model parameters as well as an accurate initial condition of the saturation. While uncertainty quantification (UQ) and parameter estimation have been used to predict reservoir parameters [55, 66, 67], unfortunately it is not feasible to obtain accurate microscope data of saturation and pressure at a particular time slice. Nonetheless, a coarse scale approximation of the saturation and pressure field can be obtained using seismic waves data and well logs data. In this work, we consider a simple two-phase model (3.7) and (3.8), and inject these coarse-scale data directly into a system via our proposed data assimilation algorithm to control the error of the solution without using any microscope initial condition.

1.3. Main result of this paper. While two-phase models have a long history of success on certain problems, they tend to lose accuracy on more complicated problems due to the insufficient and inaccurate knowledge of the initial state. Meanwhile, continuous data assimilation (DA) has recently been used to improve accuracy by incorporating measurement data into the simulation. In this work, we introduce a data assimilation model (4.1) which combines the coarse grid saturation measurement data with the multi-phase flow problem. For illustrative purpose, instead of a general multi-phase flow model, we only focus on an immiscible incompressible two-phase flow model (3.7) and (3.8). After performing an error analysis for the data assimilation algorithm, we prove an exponentially decaying error bound between the exact and approximate solutions until the error reaches a certain level (Theorem 4.3). More precisely, for a given data resolution H , we find t_0 in terms of H such that synchronization is guaranteed for all $t < t_0$ for large enough $\mu \sim \mathcal{O}(1/H)$. In this case, coarser data resolution leads to a smaller t_0 and vice versa.

In addition, we illustrate the efficiency of the algorithm by extensive computational studies. We find that the nudging algorithm achieves synchronization with data that is much more coarser than required by the rigorous estimates in Theorem 4.3. Furthermore, we demonstrate numerically that observation on a small fraction of the domain suffices for global assimilation, which may in practice indeed be the case for data collected on the smaller portion of the whole domain.

Organization of this paper. In section 2, we briefly introduce basic notations and preliminaries used in the analysis. Section 3 provides background on the two-phase model and

revisits the existence and uniqueness argument of the model. Later, in section 4, after introducing the data assimilation algorithm, we state and prove our main results. We give conditions under which the approximate solution, obtained by the data assimilation algorithm, converges to the solution of the two-phase model. In section 5, we present numerical results to demonstrate the performance of our proposed data assimilation model.

2. NOTATION AND PRELIMINARIES

Let $\Omega \subset \mathbb{R}^d$ be a bounded open domain. From what follows, we always write C as a generic positive constant independent of the model parameters. Let $p \in [1, \infty]$, and the Lebesgue space $L^p(\Omega)$ is the space of all measurable functions \mathbf{v} on Ω with which

$$\|\mathbf{v}\|_{L^p} := \left(\int_{\Omega} |\mathbf{v}(\mathbf{x})|^p d\mathbf{x} \right)^{\frac{1}{p}} < \infty, \quad \text{if } p \in [1, \infty),$$

$$\|\mathbf{v}\|_{L^\infty} := \text{ess-sup}_{\mathbf{x} \in \Omega} |\mathbf{v}(\mathbf{x})| < \infty, \quad \text{if } p = \infty.$$

The L^2 norm and inner product will be denoted by $\|\cdot\|$ and (\cdot, \cdot) respectively, while all other norms will be labeled with subscripts. Let \mathbf{V} be a Banach space of functions defined on Ω with the associated norm $\|\cdot\|_{\mathbf{V}}$. We denote by $L^p(a, b; \mathbf{V})$, $p \in [1, \infty]$, the space of functions $\mathbf{v} : (a, b) \rightarrow \mathbf{V}$ such that

$$\|\mathbf{v}\|_{L^p(a, b; \mathbf{V})} := \left(\int_a^b \|\mathbf{v}(t)\|_{\mathbf{V}}^p dt \right)^{\frac{1}{p}} < \infty, \quad \text{if } p \in [1, \infty),$$

$$\|\mathbf{v}\|_{L^\infty(a, b; \mathbf{V})} := \text{ess-sup}_{t \in (a, b)} \|\mathbf{v}(t)\|_{\mathbf{V}} < \infty, \quad \text{if } p = \infty.$$

From now on, for notational sake, we will denote an integral of a function f over a domain Ω with one of the following three notations if no confusion will arise

$$\int_{\Omega} f(x) dx, \quad \int_{\Omega} f dx, \quad \text{and} \quad \int_{\Omega} f.$$

In addition, we consider

$$V_0 = \{v \in H^1(\Omega) \mid \int_{\Omega} v = 0\},$$

$$V_0^* = \{v \in H^{-1}(\Omega) \mid \int_{\Omega} v = 0\}.$$

Definition 2.1. The bi-linear operator $a(\cdot, \cdot)$ and semi-norm $|\cdot|_K$ are given as

$$a(u, v) = \int_{\Omega} K \nabla u \cdot \nabla v, \quad \forall u, v \in H^1(\Omega),$$

and

$$|u|_K^2 = a(u, u),$$

where K is a tensor with $K_{ij} \in L^\infty(\Omega)$.

Remark 2.1. Note that $|\cdot|_K$ defines a norm for V_0 .

Definition 2.2. The Green's operator $G : V_0^* \rightarrow V_0$ is given by

$$a(G(u), v) = (u, v).$$

We define the norms of V_0 and V_0^* respectively as $\|v\|_{V_0} = |v|_K$ and $\|u\|_{V_0^*} := \|G(u)\|_{V_0}$ for all $u \in V_0^*, v \in V_0$.

Our data assimilation method requires that the observational measurements $\Pi_H(\mathbf{u})$, be given as linear interpolant observables, satisfying $\Pi_H : L^2(\Omega) \rightarrow L^2(\Omega)$ such that

$$(2.1) \quad \begin{aligned} \|\Pi_H \varphi\| &\leq c_I \|\varphi\|, & \forall \varphi \in L^2(\Omega), \\ \|\varphi - \Pi_H \varphi\| &\leq c_0 H \|\varphi\|_{H^1(\Omega)}, & \forall \varphi \in H^1(\Omega). \end{aligned}$$

An example of such interpolation operators can be given by a projection operator onto the Fourier modes with wave numbers $|k| \leq 1/H$. Other physical examples include the volume elements and constant finite element interpolation [53].

3. A SIMPLE TWO-PHASE FLOW MODEL

In this section, we describe an immiscible incompressible two-phase flow model. In this model, the flow of the fluids is governed by the Darcy's law of the water and the oil phases. More precisely, the velocity \tilde{v}_α of phase α is described as

$$\tilde{v}_\alpha = -\frac{k_{r\alpha}}{\mu_\alpha} K \nabla P_\alpha, \quad \text{in } (0, T) \times \Omega, \quad \alpha = o \text{ (oil), } w \text{ (water)},$$

where $k_{r\alpha}, \mu_\alpha, P_\alpha$, and ρ_α are the relative permeability, viscosity, pressure, and density of phase α , K is the absolute permeability, T is the final time and Ω is the reservoir domain. We consider the capillary pressure P_{cow} defined as

$$P_{cow} := P_o - P_w.$$

The saturation of phase α , denoted by S_α , is governed by the mass balance equation

$$\frac{\partial(\phi \rho_\alpha S_\alpha)}{\partial t} + \nabla \cdot (\rho_\alpha \tilde{v}_\alpha) = \rho_\alpha \tilde{q}_\alpha, \quad \text{in } (0, T) \times \Omega, \quad \alpha = o, w,$$

where \tilde{q}_α is the volumetric input of phase α and ϕ is the porosity of the medium. The saturation S_α then satisfies

$$(3.1) \quad S_o + S_w = 1.$$

To simplify the model, in our work, we only consider the case when the density ρ_α , the viscosity μ_α , and the porosity ϕ are constant functions, and that the relative permeability $k_{r\alpha}$, the capillary pressure P_{cow} are functions only depending on S_α . Using (3.1), we have $S_o = 1 - S_w$ and therefore $k_{r\alpha}$ and P_{cow} can be written as a function of S_w . We then define the function κ_α as

$$\kappa_\alpha(S_w) = \frac{k_{r\alpha}(S_w)}{\phi \mu_\alpha}.$$

To simplify the notation, we will omit the sub-index w and denote S_w as S in the following discussion,. We furthermore assume $\kappa_\alpha \in L^\infty(0, 1)$, K is a L^∞ positive tensor and

$$\infty > \bar{\kappa} \geq (\kappa_w(S_w) + \kappa_o(S_w)) \geq \underline{\kappa} > 0,$$

$$\infty > \overline{K} \geq \xi^T K \xi \geq \underline{K} > 0 \quad \forall \xi \in \mathbb{R}^d, \|\xi\| = 1,$$

for some constants $\underline{\kappa}$, $\overline{\kappa}$, \underline{K} , and \overline{K} . Since ϕ , ρ_α are constants, the mass balance equations can be simplified as

$$(3.2) \quad \frac{\partial(S_\alpha)}{\partial t} + \nabla \cdot (v_\alpha) = q_\alpha, \text{ in } (0, T) \times \Omega, \quad \alpha = o, w,$$

where $q_\alpha = \frac{\tilde{q}_\alpha}{\phi}$ and

$$v_\alpha = -\kappa_\alpha K \nabla P_\alpha, \text{ in } (0, T) \times \Omega, \quad \alpha = o, w.$$

We then obtain a pressure equation by summing the equations (3.2)

$$(3.3) \quad -\nabla \cdot \left(K(\kappa_o(\nabla P_o) + \kappa_w(\nabla P_w)) \right) = \nabla \cdot (v_o + v_w) = q_o + q_w.$$

With this, the system can be simplified to

$$(3.4) \quad -\nabla \cdot ((\kappa_w + \kappa_o)K \nabla P_w) = q_t + \nabla \cdot (\kappa_o \nabla P_{cow}),$$

$$(3.5) \quad \frac{\partial(S_w)}{\partial t} - \nabla \cdot (\kappa_w K \nabla P_w) = q_w,$$

where $q_t = q_o + q_w$.

Global pressure. We recall how to reformulate the equations with the help of the concept of global pressure. We assume $\beta = -\frac{\partial P_{cow}}{\partial S_w} > 0$. The global pressure P is defined as

$$P(S, t, x) = P_o(t, x) + \int_0^S f_w \beta(\xi) d\xi,$$

where $f_i = \frac{\kappa_i}{\kappa}$ and $\kappa = \sum_{i=o,w} \kappa_i$ and $S = S(t, x)$ is a function of (t, x) . In case there will not cause any confusion, we would, by an abuse of notation, simplify $p(S(t, x), t, x)$ as $p(t, x)$. We may then check directly that

$$\nabla \left(\int_0^S f_w \beta(\xi) d\xi \right) = f_w \beta \nabla S = -f_w \nabla P_{cow}.$$

Hence, we have $\kappa \nabla P = \kappa \nabla P_o - \kappa_w \nabla P_{cow} = \kappa_o \nabla P_o + \kappa_w \nabla P_w$.

Now define a function θ as

$$(3.6) \quad \theta(S) := \int_0^S \frac{\kappa_w(\xi) \kappa_o(\xi)}{\kappa(\xi)} \beta(\xi) d\xi,$$

which is monotone since $\frac{\kappa_w(\xi) \kappa_o(\xi)}{\kappa(\xi)} \beta(\xi) > 0$ and obtain

$$\kappa(S) \nabla \theta(S) = \kappa_w(S) \kappa_o(S) \beta(S) \nabla S = -\kappa_w(S) \kappa_o(S) \nabla P_{cow}(S).$$

We therefore have

$$\begin{aligned} \nabla \theta + \kappa_w \nabla P &= -\frac{\kappa_o \kappa_w}{\kappa} \nabla P_{cow} + \frac{\kappa_o \kappa_w}{\kappa} \nabla P_o + \frac{\kappa_w^2}{\kappa} \nabla P_w \\ &= \kappa_w \nabla P_w = -K^{-1} v_w \end{aligned}$$

and

$$\begin{aligned} -\nabla\theta + \kappa_o \nabla P &= \frac{\kappa_o \kappa_w}{\kappa} \nabla P_{cow} + \frac{\kappa_o^2}{\kappa} \nabla P_o + \frac{\kappa_o \kappa_w}{\kappa} \nabla P_w \\ &= \kappa_o \nabla P_o = -K^{-1} v_o. \end{aligned}$$

This leads to the equation

$$-\nabla(\kappa(S)K(x)\nabla P(t, x)) = q_t(x), \quad \forall x \in \Omega,$$

where $q_t = q_o + q_w$. We then define an inverse map \mathbb{T} of θ , such that

$$\mathbb{T}(\theta(S)) = S.$$

We notice that \mathbb{T} is well-defined and θ is irreversible since θ is monotone. With the help of the aforementioned notations, the system can be now rewritten as: find the solution pair (p, S) satisfying

$$(3.7) \quad -\nabla(\kappa K \nabla P) = q_t,$$

$$(3.8) \quad \partial_t(S) - \nabla \cdot (K \nabla \theta(S) + \kappa_w K \nabla P) = q_w.$$

3.1. Analysis of the two-phase model; Existence and Uniqueness results. In this subsection, we first revisit some classical results of the two-phase model, and then review the existence and uniqueness results of the weak solution of the problems (3.7) and (3.8) as in [2, 3, 5, 19, 24]. The remaining analysis is proceed with the following common assumptions [24, 75].

A1. $\Omega \subset \mathbb{R}^d$ for $d \in \{2, 3\}$ is a connected Lipschitz domain.

A2. κ_α are continuous and $\kappa_w(0) = \kappa_o(0) = 0$

$$\kappa_o(S_o) > 0 \text{ if } S_o > 0,$$

$$\kappa_w(S_w) > 0 \text{ if } S_w > 0.$$

A3. $q_w, q_o \in L^\infty(0, T; H^{-1}(\Omega))$.

A4. κ_w and κ_o satisfy

$$\kappa_w(S) = C_w S^{1+\xi_w},$$

$$\kappa_o(S) = C_o (1 - S)^{1+\xi_o},$$

for some $\xi_o, \xi_w, C_w, C_o > 0$.

A5. Denote $b(S) = \frac{\kappa_w(S)\kappa_o(S)}{\kappa(S)}\beta(S)$, and then $b(S) \leq C_0$ for all $0 \leq S \leq 1$.

A6. $\beta(S)$ satisfies the bound

$$c_\alpha(S)^{-\beta_w} (1 - S)^{-\beta_o} \leq \beta(S) \leq C_\alpha(S)^{-\beta_w} (1 - S)^{-\beta_o},$$

for some $\beta_o, \beta_w, C_\alpha, c_\alpha > 0$.

A7. κ satisfies the inequality

$$|\kappa(S_2) - \kappa(S_1)| \leq C(\theta(S_2) - \theta(S_1), S_2 - S_1)^{\frac{1}{2}}, \quad \text{for } S_1, S_2 \in [0, 1].$$

A8. $p \in L^\infty(0, T; W^{1,\infty}(\Omega))$.

Remark 3.1. Assumption A8 can also be derived directly from some mild assumptions given in [24, 75].

Proposition 3.2. *With assumptions A4 – A6, there are positive constants $\delta < 1/2$, $\tau_i > 0$ and $C_i > 0$ such that*

$$\begin{aligned} C_1 S^{\tau_w} &\leq b(S) \leq C_2 S^{\tau_w}, & S \in [0, \delta], \\ C_3 &\leq b(S) \leq C_4, & S \in [\delta, 1 - \delta], \\ C_5(1 - S)^{\tau_o} &\leq b(S) \leq C_6(1 - S)^{\tau_o}, & S \in [1 - \delta, 1], \end{aligned}$$

where $\tau_w = 1 + \xi_w - \beta_w$, and $\tau_o = 1 + \xi_o - \beta_o$.

With the aforementioned assumptions, we arrive at the following lemma, which will be important for our subsequent analysis.

Lemma 3.3. *Assuming A4 – A6, for any $S_1, S_2 \in [0, 1]$, then we have*

$$\tilde{C}(S_2 - S_1)^{2+\tau} \leq (\theta(S_2) - \theta(S_1))(S_2 - S_1) \leq C_0(S_2 - S_1)^2$$

where $\tau = \max(\tau_w, \tau_o)$.

Proof. Without loss of generality, assume $S_2 \geq S_1$, then by the definition of θ in (3.6), we have

$$\begin{aligned} (\theta(S_2) - \theta(S_1)) &= \int_{S_1}^{S_2} b(S) dS \leq C_0 \int_{S_1}^{S_2} dS, \\ (\theta(S_2) - \theta(S_1)) &\geq c \int_{S_1}^{S_2} (1 - S)^{\tau_o} S^{\tau_w}, \end{aligned}$$

and therefore

$$\tilde{C}(S_2 - S_1)^{1+\tau} \leq |\theta(S_2) - \theta(S_1)| \leq C_0(S_2 - S_1).$$

□

We now state the well-posedness result for the model (3.7) and (3.8), equipped with Neumann boundary conditions for P and S and initial condition for S , although the results can be extended to more general boundary conditions. The complete proof can be found in the above mentioned references. Since some of the proofs are related to the techniques we used in our main theorem, we will put the proof of some lemmas in the appendix. Readers may refer to [24] for further details.

Theorem 3.4 (Existence and uniqueness of weak solutions of the two-phase flow model). [24] *Let $\Omega \subset \mathbb{R}^d$ for $d \in \{2, 3\}$ be a connected Lipschitz domain. Assume $S(0, \cdot) \in L^2(\Omega)$, S and P with homogeneous Neumann boundary conditions in (3.7) and (3.8). Problems (3.7) and (3.8) have a unique weak solution satisfying for all $T > 0$*

$$\partial_t S_w \in L^2(0, T; H^{-1}(\Omega)).$$

Moreover

$$(3.9) \quad \begin{aligned} \int_{\Omega} \kappa(S_w) K \nabla P \cdot \nabla w &= \int_{\Omega} q_t w, \quad \forall w \in H^1(\Omega), \\ \int_0^T \int_{\Omega} \left(\partial_t S_w v + K(\nabla \theta(S_w) + \kappa_w \nabla P) \cdot \nabla v \right) &= \int_0^T \int_{\Omega} q_w v, \quad \forall v \in L^2(0, T; H^1(\Omega)). \end{aligned}$$

The proof of existence starts with defining a discrete time solution of the problem. Denote

$$\partial^n v(t) = \frac{v(t + \eta) - v(t)}{\eta},$$

for any function $v(t)$, where $\eta = T/N$. Next define

$$I_{i,\eta}(V) = \left\{ v \in L^\infty(0, T; V) : v \text{ is piece-wise polynomial with degree } i \text{ in time on each sub-interval } J_i \subset J \right\},$$

where $J_i = (t_i, t_{i+1}]$, $t_i = i\eta$ and $t_N = T$. We then define the discrete time solution $P^\eta \in I_{0,\eta}(H^1(\Omega))$ with

$$\int_{\Omega} P^\eta(t, \cdot) = 0, \quad \text{and} \quad \theta^\eta \in I_{1,\eta}(H^1(\Omega)),$$

which satisfy

(3.10)

$$\begin{aligned} \int_0^T \int_{\Omega} \kappa(S_w) K \nabla P^\eta \cdot \nabla w &= \int_0^T \int_{\Omega} q_t w \quad \forall w \in I_{0,h}(H^1(\Omega)), \\ \int_0^T \int_{\Omega} \left(\partial^n(T(\theta^\eta))v + \kappa_w K \nabla P^\eta \cdot \nabla v + K \nabla \theta^\eta \cdot \nabla v \right) &= \int_0^T \int_{\Omega} q_w v \quad \forall v \in I_{0,h}(H^1(\Omega)). \end{aligned}$$

We now need the following result, which are stated without proof.

Lemma 3.5. [24] *The discrete problems (3.10) are well-posed.*

Lemma 3.6. [24] *Let $d : \mathbb{R} \rightarrow \mathbb{R}$ be an increasing function such that $d(0) = 0$ and $\{c_i\}$ be a sequence of real numbers. Then for any number $m > 0$,*

$$\sum_{k=1}^m (d(c_k) - d(c_{k-1}))c_k \geq D(c_m) - D(c_0) \geq -D(c_0)$$

where

$$D(c) = \int_0^c (d(c) - d(\xi))d\xi.$$

Next, we recall the following Lemma, which is important to our subsequent analysis.

Lemma 3.7. [24] *The discrete solution P^η , θ^η satisfy*

$$\|P^\eta\|_{L^\infty(0,T;H^1(\Omega))} + \|\theta^\eta\|_{L^2(0,T;H^1(\Omega))} \leq C,$$

where C is independent of η .

From Lemma 3.6, and since P^η and θ^η remain bounded, we have the following corollary.

Corollary 3.8. [24] *Let P^η and θ^η be solutions to (3.10), then*

- (1) *For any $2 \leq r < \infty$, there exists a subsequence $P^\eta \rightharpoonup p$ weakly in $L^r(0, T; H^1(\Omega))$, and $\theta^\eta \rightharpoonup \theta$ weakly in $L^2(0, T; H^1(\Omega))$.*
- (2) *There is a subsequence $\theta^\eta \rightarrow \theta$ strongly in $L^2(0, T; L^2(\Omega))$.*

(3) There is a subsequence $\theta^n \rightarrow \theta$ strongly in $L^2(0, T; H^{1-\alpha})$ for any $0 < \alpha < 1/2$, and $S^n \rightarrow S$ pointwise a.e. on $(0, T] \times \Omega$ where $S^n = T(\theta^n)$.

In the rest of this section, we analyze the stability of the weak solution by bounding the difference between the two solutions (S_i, P_i) , $i = 1, 2$ as follows.

Lemma 3.9. [24] *Let (S_i, P_i) , $i = 1, 2$ be two weak solutions to (3.9) given by Theorem 3.4 with source term $q_{t,i}$ and $q_{w,i}$ with respectively. Then we have*

$$\|\nabla(P_2 - P_1)\|_{L^2} \leq C (\|\kappa(S_2) - \kappa(S_1)\|_{L^2} + \|q_{t,2} - q_{t,1}\|_{L^2}).$$

With π to be the average operator $\pi(u) = \frac{1}{|\Omega|} \int_{\Omega} u$, and $e = (I - \pi)(S_2 - S_1)$, where s_1 and s_2 are solutions with two different sources, one can prove the following stability result.

Lemma 3.10. [24] *Let (S_i, P_i) , $i = 1, 2$ be two weak solutions to (3.9) given by Theorem 3.4 with source term $q_{t,i}$ and $q_{w,i}$ with respectively. With the assumptions A1 – A8, we have*

$$\begin{aligned} & \frac{1}{2} \partial_t \int_0^t \|e\|_{V_0^*}^2 + \int_0^t (\theta_2 - \theta_1, S_2 - S_1) \\ & \leq \frac{\delta_p^p}{p} \int_0^t \|S_1 - S_2\|_{L^p}^p + \frac{C_q}{q \delta_p^q} \left(\|\pi(S_2 - S_1)(0, \cdot)\|_{L^q}^q + \|q_{w,2} - q_{w,1}\|_{L^q(0,t;L^q)}^q \right) \\ & \quad + C \frac{\delta}{2} \int_0^t \left(\|\kappa(S_2) - \kappa(S_1)\|_{L^2}^2 + \|\nabla(P_2 - P_1)\|_{L^2}^2 + \|q_{w,2} - q_{w,1}\|_{L^2}^2 \right) + C \frac{1}{2\delta} \int_0^t \|\nabla G(e)\|_{L^2}^2 \end{aligned}$$

where δ, δ_p are arbitrary positive constants, p is arbitrary positive constant larger than 1 and $\frac{1}{p} + \frac{1}{q} = 1$.

We will give the stability estimate and thus the uniqueness with the following theorem.

Theorem 3.11. [24] *Let (S_i, P_i) , $i = 1, 2$ are two weak solutions to (3.9) given by Theorem 3.4. With the assumptions A1 – A8, we have*

$$\begin{aligned} \|(I - \pi)(S_2 - S_1)\|_{L^\infty(0,T;V_0^*)}^2 & \leq C e^{Ct} \left(\|\pi(S_2 - S_1)(0, \cdot)\|_{L^{q_0}(\Omega)}^{q_0} + \|q_{w,2} - q_{w,1}\|_{L^{q_0}(0,T;L^{q_0}(\Omega))}^{q_0} \right. \\ & \quad \left. + \|(I - \pi)(S_2 - S_1)(0, \cdot)\|_{V_0^*}^2 + \|q_{w,2} - q_{w,1}\|_{L^2(0,T;L^2(\Omega))}^2 + \|q_{t,2} - q_{t,1}\|_{L^2(0,T;L^2(\Omega))}^2 \right), \end{aligned}$$

for some $C > 0$, τ defined as in Lemma 3.3, and $q_0 = \frac{2 + \tau}{1 + \tau}$.

4. DATA ASSIMILATION ALGORITHM FOR THE TWO-PHASE FLOW PROBLEM

In this section, we first describe the nudging algorithm for the two-phase flow equations (3.7) and (3.8). We can consider we can obtain some observed data of the saturation. We consider the data collecting operator is denoted as $\Pi_H^*(S)$. We remarked that the image of the data collecting operator is usually in a finite dimension space. The data assimilation

algorithm for two-phase flow problem is defined as

$$(4.1) \quad \begin{aligned} & -\nabla \cdot (\kappa K \nabla P) = q_t, \\ & \frac{\partial(\tilde{S})}{\partial t} + \nabla \cdot \left(\frac{\kappa_w}{\kappa} K \nabla P \right) + \mu (\Pi_H^*(\tilde{S}) - \Pi_H^*(S)) = q_w, \end{aligned}$$

where $\Pi_H : H^1(\Omega) \rightarrow L^2(\Omega)$ is a linear interpolant operator satisfying

$$(4.2) \quad \begin{aligned} \|\Pi_H(S) - S\| &\leq CH \|S\|_{H^1}, \\ \|\Pi_H(S)\| &\leq C \|S\|, \end{aligned}$$

which can naturally be extended to $L^2(\Omega)$. The dual operator is given by $\Pi_H^* : L^2(\Omega) \rightarrow H^{-1}(\Omega)$

$$\int_{\Omega} \Pi_H(S) v = \int_{\Omega} S \Pi_H^*(v), \quad \forall v \in L^2(\Omega).$$

For instance, Π_H may be considered to be the L^2 projection operator to the piece-wise constant finite element space (for more details see [53]), namely,

$$\Pi_H(S)(x) = \int_{K_i} S, \quad \forall x \in K_i,$$

where K_i is a coarse element in \mathcal{T}_H , and in this case, we have

$$(4.3) \quad \Pi_H^* = \Pi_H.$$

In this case, the domain Ω is partitioned into a coarse partition \mathcal{T}_H , where the observed data are collected. More precisely, we collect the data of the averaged water saturation S in each coarse element containing $\{x_i\}_i^M \subset \Omega$, where x_i are the points that physical measurements are performed where M is the number of measurements. For example, we can consider the $\{x_i\}_i^M \subset \Omega$ to be all of the center point of the coarse grid element.

Remark 4.1. We remark that there are many choices of Π_H , for example, we can consider Π_H as a standard polynomial interpolation operator .

Definition 4.1 (Weak solution to the data assimilation algorithm). Let (S, P) be the solution to the two-phase problem from Theorem 3.4. The continuous data assimilation equations (4.1) has a unique weak solutions (\tilde{S}, \tilde{P}) that satisfies for all $T > 0$

$$\partial_t \tilde{S} \in L^2(0, T; H^{-1}(\Omega))$$

and

$$(4.4) \quad \begin{aligned} & \int_{\Omega} \kappa(\tilde{S}) K \nabla \tilde{P} \cdot \nabla w = \int_{\Omega} q_t w, \quad \forall w \in H^1(\Omega), \\ & \int_0^T \int_{\Omega} \left(\partial_t \tilde{S} v + K(\nabla \tilde{\theta}(\tilde{S}) + \kappa_w(\tilde{S}) \nabla \tilde{P}) \cdot \nabla v + \mu \Pi_H^*(\tilde{S} - S)(v) \right) \\ & \qquad \qquad \qquad = \int_0^T \int_{\Omega} q_w v, \quad \forall v \in L^2(0, T; H^1(\Omega)). \end{aligned}$$

Remark 4.2. Although the well-posedness of (4.4) is not the focus of this work, we speculate that it can be proved by a usual compactness argument [24], or by the fixed-point argument which has recently been suggested in [21] for a similar problem.

In the next theorem, we analyze the residual error coming from the data assimilation algorithm with unknown initial condition, which is the main analytical result of this work.

Theorem 4.3. *Let $\Omega \subset \mathbb{R}^d$ for $d \in \{2, 3\}$ be a connected Lipschitz domain. Consider S be a solution of the two-phase equations with initial data $S(0) \in L^2(\Omega)$, ensured by Theorem 3.4, and $\Pi_H : L^2(\Omega) \rightarrow L^2(\Omega)$ be a linear map satisfying (2.1). Let \tilde{S} be a solution to the data assimilation algorithm given by (4.1) with homogeneous Neumann boundary conditions. Then for all $H > 0$, if*

$$(4.5) \quad \mu := \mu(\tilde{\gamma}, \tilde{C}, C_2, H) = 2\tilde{\gamma} \left(\frac{C_2}{\tilde{C}} \right)^{-\frac{1}{2}} H^{-1} = O(H^{-1}),$$

the following bound holds for $t < t_0$

$$(4.6) \quad \|(I - \pi)(\tilde{S} - S)\|_{V_0^*}^2 \leq e^{-\frac{\mu}{2}t} \left(\|e(0, \cdot)\|_{V_0^*}^2 + 2C_5 \|\pi(\tilde{S} - S)(0, \cdot)\|_{L^{q_0}}^{q_0} \right),$$

where $t_0 := t_0(\tilde{\gamma}, \tilde{C}, C_2, H)$ is given as

$$(4.7) \quad t_0 = \max \left\{ 0 \leq \zeta < T, \text{ s.t. } c^* H^{2+\tau} \leq \|\tilde{S}(t) - S(t)\|_{L^{2+\tau}}^{2\tau+\tau^2}, \forall 0 \leq t \leq \zeta \right\}.$$

Herein, \tilde{C} , C_2 , C_5 are constants, defined in the proof of this theorem, depending only on Ω , and $c^* := c^*(\tilde{\gamma}, \tilde{C}, C_2)$ is a constant appearing in (4.15), whereas $\tilde{\gamma} = O(1)$ with respect to H .

Remark 4.4. The above theorem showed that if we choose $\mu = O(H^{-1})$, the error of the solution will decay exponentially until the error is reduced to a certain level.

Proof. Subtracting (3.9) and (4.4), the difference satisfies the following error equations

$$(4.8) \quad \int_{\Omega} \kappa(\tilde{S}) K \nabla(\tilde{P} - P) \cdot \nabla w = \int_{\Omega} \left(\kappa(S) - \kappa(\tilde{S}) \right) K \nabla P \cdot \nabla w, \quad \forall w \in H^1(\Omega),$$

$$(4.9) \quad \begin{aligned} & \int_0^T \int_{\Omega} \left(\partial_t(\tilde{S} - S)v + K \nabla(\tilde{\theta} - \theta) \cdot \nabla v + \kappa_w(\tilde{S}) K \nabla(\tilde{P} - P) \cdot \nabla v + \mu(\tilde{S} - S) \Pi_H(v) \right) \\ & = \int_0^T \int_{\Omega} \left(\kappa_w(S) - \kappa_w(\tilde{S}) \right) K \nabla P \cdot \nabla v, \quad \forall v \in L^2(0, T; H^1(\Omega)). \end{aligned}$$

Denote $e = (I - \pi)(\tilde{S} - S)$ and set $v = G(e)$ in (4.9). With that, we obtain

$$(4.10) \quad \begin{aligned} & \int_0^T \int_{\Omega} \left(\partial_t(\tilde{S} - S)G(e) + K \nabla(\tilde{\theta} - \theta) \cdot \nabla G(e) + \mu(\tilde{S} - S) \Pi_H(G(e)) \right) \\ & = \int_0^T \int_{\Omega} \left(\left(\kappa_w(S) - \kappa_w(\tilde{S}) \right) K \nabla P \cdot \nabla G(e) - \kappa_w(\tilde{S}) K \nabla(\tilde{P} - P) \cdot \nabla G(e) \right). \end{aligned}$$

With a similar argument in the proof of Lemma 3.10, we obtain

$$(4.11) \quad \int_{\Omega} \partial_t(\tilde{S} - S)G(e) = \frac{1}{2} \partial_t \|G(e)\|_V^2 = \frac{1}{2} \partial_t \|e\|_{V^*}^2,$$

and

$$(4.12) \quad \int_{\Omega} K \nabla(\tilde{\theta} - \theta) \cdot \nabla G(e) = (\tilde{\theta} - \theta, \tilde{S} - S) - (\tilde{\theta} - \theta, \pi(\tilde{S} - S)).$$

Then choose a test function $v = p(\pi(\tilde{S} - S))^{p-1}$ in (4.9) to get

$$\|\pi(\tilde{S} - S)(t, \cdot)\|_{L^p(\Omega)}^p + p\mu \int_0^t \|\pi(\tilde{S} - S)\|_{L^p(\Omega)}^p = \|\pi(\tilde{S} - S)(0, \cdot)\|_{L^p(\Omega)}^p,$$

and

$$\|\pi(\tilde{S} - S)(t, \cdot)\|_{L^p(\Omega)}^p = e^{-p\mu t} \|\pi(\tilde{S} - S)(0, \cdot)\|_{L^p(\Omega)}^p,$$

for any $p > 1$. For any $u \in V^*$, we have

$$\begin{aligned} \int_{\Omega} K \nabla G(u) \cdot \nabla G(u) &= \int_{\Omega} G(u)(u) = \int_{\Omega} (I - \Pi_H)G(u)(u) + \int_{\Omega} \Pi_H G(u)(u) \\ &\leq \bar{C}^{\frac{1}{2}} H \|K^{\frac{1}{2}} \nabla G(u)\|_{L^2} \|u\|_{L^2} + \int_{\Omega} \Pi_H G(u)(u). \end{aligned}$$

We hence obtain

$$(4.13) \quad \|u\|_{V_0^*}^2 \leq \bar{C} H^2 \|u\|_{L^2}^2 + 2 \int_{\Omega} \Pi_H G(u)(u).$$

Combining (4.11), (4.12) and (4.13) with (4.10), we have

$$\begin{aligned} &\int_0^t \left(\frac{1}{2} \partial_t \|e\|_{V_0^*}^2 + (\tilde{\theta} - \theta, \tilde{S} - S) + \frac{\mu}{2} \|K^{\frac{1}{2}} \nabla G(e)\|_{L^2}^2 \right) \\ &\leq \int_0^t \left(\frac{1}{2} \partial_t \|e\|_{V_0^*}^2 + (\tilde{\theta} - \theta, \tilde{S} - S) + \mu \int_{\Omega} \Pi_H G(e)(e) + \frac{\mu \bar{C}}{2} H^2 \|e\|_{L^2}^2 \right) \\ &= \int_0^T \int_{\Omega} \left((\kappa_w(S) - \kappa_w(\tilde{S})) K \nabla P \cdot \nabla G(e) - \kappa_w(\tilde{S}) K \nabla (\tilde{P} - P) \cdot \nabla G(e) \right. \\ &\quad \left. + (\tilde{\theta} - \theta, \pi(\tilde{S} - S)) + \frac{\mu \bar{C}}{2} H^2 \|e\|_{L^2}^2 \right) \\ &\leq C_1 \int_0^t \left((\|S - \tilde{S}\|_{L^p} + \|K^{\frac{1}{p}} \nabla (\tilde{P} - P)\|_{L^p(\Omega)}) \|K^{\frac{1}{q}} \nabla G(e)\|_{L^q} \right. \\ &\quad \left. + \|\tilde{\theta} - \theta\|_{L^{\bar{q}}} \|\pi(\tilde{S} - S)\|_{L^{\bar{p}}} + \frac{\mu \bar{C}}{2} H^2 \|e\|_{L^2}^2 \right), \end{aligned}$$

for any $p > 1$ with $\frac{1}{p} + \frac{1}{q} = 1$ and an arbitrary $\mu > 0$ which will be determined later. With an argument similar to the proof of Lemma 3.9, we can also obtain

$$\|K^{\frac{1}{p}} \nabla (\tilde{P} - P)\|_{L^p}^p \leq \hat{C}_p \|\tilde{S} - S\|_{L^p}^p.$$

hence, with $p = 2 = q$, we have

$$\begin{aligned}
(4.14) \quad & \int_0^t \left(\frac{1}{2} \partial_t \|e\|_{V_0^*}^2 + (\tilde{\theta} - \theta, \tilde{S} - S) + \frac{\mu}{2} \|K^{\frac{1}{2}} \nabla G(e)\|_{L^2}^2 \right) \\
& \leq C_1 \int_0^t \left((\|S - \tilde{S}\|_{L^2} + \|K^{\frac{1}{2}} \nabla(\tilde{P} - P)\|_{L^2(\Omega)}) \|K^{\frac{1}{2}} \nabla G(e)\|_{L^2} \right. \\
& \quad \left. + \|\tilde{\theta} - \theta\|_{L^{2+\tau}} \|\pi(\tilde{S} - S)\|_{L^{q_0}} + \frac{\mu \bar{C}}{2} H^2 \|e\|_{L^2}^2 \right),
\end{aligned}$$

where $q_0 = \frac{2+\tau}{1+\tau}$, and

$$\int_0^t \left(\|S - \tilde{S}\|_{L^2} + \|K^{\frac{1}{2}} \nabla(\tilde{P} - P)\|_{L^2(\Omega)} \right) \|K^{\frac{1}{2}} \nabla G(e)\|_{L^2} \leq \frac{\mu}{4C_1} \|K^{\frac{1}{2}} \nabla G(e)\|_{L^2}^2 + \frac{2C_2}{\mu} \|S - \tilde{S}\|_{L^2}^2,$$

where $C_2 := 4C_1(1 + \hat{C}_2)$. We next estimate the term $\|\tilde{\theta} - \theta\|_{L^{2+\tau}} \|\pi(\tilde{S} - S)\|_{L^{q_0}}$ as

$$\begin{aligned}
\|\tilde{\theta} - \theta\|_{L^{2+\tau}} \|\pi(\tilde{S} - S)\|_{L^{q_0}} & \leq \frac{\tilde{C}}{2C_1 C_0} \|\tilde{\theta} - \theta\|_{L^{2+\tau}}^{2+\tau} + \frac{2C_1 C_0 (1 + \tau)}{\tilde{C} (2 + \tau)^2} \|\pi(\tilde{S} - S)\|_{L^{q_0}}^{q_0} \\
& \leq \frac{\tilde{C}}{2C_1} \|\tilde{S} - S\|_{L^{2+\tau}}^{2+\tau} + \frac{C_3}{C_1} \|\pi(\tilde{S} - S)\|_{L^{q_0}}^{q_0},
\end{aligned}$$

where $C_3 = \frac{2C_1^2 C_0 (1 + \tau)}{\tilde{C} (2 + \tau)^2}$. Now, from $\int_0^t (\tilde{\theta} - \theta, \tilde{S} - S) \geq \tilde{C} \int_0^t \int_{\Omega} |\tilde{S} - S|^{2+\tau}$, we get that

$$\begin{aligned}
& \int_0^t \left(\frac{1}{2} \partial_t \|e\|_{V_0^*}^2 + \frac{\tilde{C}}{2} \int_0^t \int_{\Omega} |\tilde{S} - S|^{2+\tau} + \frac{\mu}{4} \|K^{\frac{1}{2}} \nabla G(e)\|_{L^2}^2 \right) \\
& \leq \int_0^t \left(\frac{C_2}{\mu} \|S - \tilde{S}\|_{L^2}^2 + C_3 \|\pi(\tilde{S} - S)\|_{L^{q_0}}^{q_0} + \frac{\mu \bar{C}}{2} H^2 \|e\|_{L^2}^2 \right),
\end{aligned}$$

Then with the help of $\|e\|_{L^2}^2 \leq \|\tilde{S} - S\|_{L^2}^2$ and $\|\pi(\tilde{S} - S)\|_{L^{q_0}}^{q_0} \leq e^{-2(q_0)t} \|\pi(\tilde{S} - S)(0, \cdot)\|_{L^{q_0}}^{q_0}$, we obtain

$$\begin{aligned}
& \int_0^t \left(\frac{1}{2} \partial_t \|e\|_{V_0^*}^2 + \frac{\tilde{C}}{2} \int_0^t \int_{\Omega} |\tilde{S} - S|^{2+\tau} + \frac{\mu}{4} \|K^{\frac{1}{2}} \nabla G(e)\|_{L^2}^2 \right) \\
& \leq \left(\frac{2C_2}{\mu} + \frac{\mu \bar{C}}{2} H^2 \right) \|S - \tilde{S}\|_{L^2}^2 + C_3 \int_0^t e^{-2(q_0)t} \|\pi(\tilde{S} - S)(0, \cdot)\|_{L^{q_0}}^{q_0}.
\end{aligned}$$

We can now take μ to be the form $\mu = 2\tilde{\gamma} \left(\frac{C_2}{\tilde{C}} \right)^{-\frac{1}{2}} H^{-1}$ (where $\tilde{\gamma}$ is a chosen constant) to get

$$\left(\frac{2C_2}{\mu} + \frac{\mu \bar{C}}{2} H^2 \right) \|S - \tilde{S}\|_{L^2}^2 = H \left(\frac{C_2}{\tilde{C}} \right)^{\frac{1}{2}} \left(\frac{1}{\tilde{\gamma}} + \tilde{\gamma} \right).$$

With $\int_0^t \int_{\Omega} |\tilde{S} - S|^2 \leq \tilde{C}_\tau \int_0^t \left(\int_{\Omega} |\tilde{S} - S|^{2+\tau} \right)^{\frac{2}{2+\tau}}$, we obtain

$$\int_0^t \left(\frac{1}{2} \partial_t \|e\|_{V_0^*}^2 + \frac{\tilde{C}}{2} \int_0^t \int_{\Omega} |\tilde{S} - S|^{2+\tau} + \frac{\mu}{4} \|K^{\frac{1}{2}} \nabla G(e)\|_{L^2}^2 \right)$$

$$\leq H \left(\frac{C_2}{\bar{C}} \right)^{\frac{1}{2}} \left(\frac{1}{\tilde{\gamma}} + \tilde{\gamma} \right) \int_0^t \left(\int_{\Omega} |\tilde{S} - S|^{2+\tau} \right)^{\frac{2}{2+\tau}} + C_3 \int_0^t e^{-2(q_0)t} \|\pi(\tilde{S} - S)(0, \cdot)\|_{L^{q_0}}^{q_0}.$$

Now consider

$$I := \left\{ 0 < t < T, \quad \text{such that} \quad c^* H^{2+\tau} \leq \left(\int_{\Omega} |\tilde{S}(t, \cdot) - s(t, \cdot)|^{2+\tau} \right)^{\tau} \right\},$$

where

$$(4.15) \quad c^* = \left(\left(\frac{C_2}{\bar{C}} \right)^{\frac{1}{2}} \left(\frac{1}{\tilde{\gamma}} + \tilde{\gamma} \right) \right)^{2+\tau} \left(\frac{\tilde{C}}{4} \right)^{-2-\tau}.$$

Now for all $t \in I$, we have

$$\left(\frac{C_2}{\bar{C}} \right)^{\frac{2+\tau}{2}} \left(\frac{1}{\tilde{\gamma}} + \tilde{\gamma} \right)^{2+\tau} \left(\frac{\tilde{C}}{4} \right)^{-2-\tau} H^{2+\tau} \leq \left(\int_{\Omega} |\tilde{S} - S|^{2+\tau} \right)^{\tau},$$

and

$$\begin{aligned} & H \left(\frac{C_2}{\bar{C}} \right)^{\frac{1}{2}} \left(\frac{1}{\tilde{\gamma}} + \tilde{\gamma} \right) \int_0^t \left(\int_{\Omega} |\tilde{S} - S|^{2+\tau} \right)^{\frac{2}{2+\tau}} \\ &= \left(\left(\frac{C_2}{\bar{C}} \right)^{\frac{2+\tau}{2}} \left(\frac{1}{\tilde{\gamma}} + \tilde{\gamma} \right)^{2+\tau} H^{2+\tau} \left(\int_{\Omega} |\tilde{S} - S|^{2+\tau} \right)^{-\tau} \right)^{\frac{1}{2+\tau}} \int_0^t \left(\int_{\Omega} |\tilde{S} - S|^{2+\tau} \right) \\ &\leq \frac{\tilde{C}}{4} \int_0^t \int_{\Omega} |\tilde{S} - S|^{2+\tau}. \end{aligned}$$

Hence, we have

$$\begin{aligned} \int_0^t \left(\frac{1}{2} \partial_t \|e\|_{V_0^*}^2 + \frac{\tilde{C}}{4} \int_{\Omega} |\tilde{S} - S|^{2+\tau} + \frac{\mu}{4} \|e\|_{V_0^*}^2 \right) &\leq C_3 \int_0^t e^{-2(q_0)t} \|\pi(\tilde{S} - S)(0, \cdot)\|_{L^{q_0}}^{q_0} \\ &\leq C_5 \|\pi(\tilde{S} - S)(0, \cdot)\|_{L^{q_0}}^{q_0}, \end{aligned}$$

which proves the theorem as

$$\|e(t, \cdot)\|_{V_0^*}^2 \leq e^{-\frac{\mu}{2}t} \left(\|e(0, \cdot)\|_{V_0^*}^2 + 2C_5 \|\pi(\tilde{S} - S)(0, \cdot)\|_{L^{q_0}}^{q_0} \right).$$

□

Remark 4.5. We remark that our method can be likewise extended to a general multi-phase model with no obstruction; however, for the sake of simplicity, we will postpone that to a future work.

5. COMPUTATIONAL STUDY

We now present results of two numerical tests that illustrate the theory given in the last section. We consider Algorithm (4.1) for two scenarios with two different permeability profiles. In both tests, the domain is $\Omega = (0, 100)^2$. In all of our numerical tests, we consider Neumann boundary conditions for P and S . The reference and the approximate solutions are calculated in a fine square mesh with fine mesh size $h = \sqrt{2}/100$ with time step size $dt = 0.05$. For the numerical method, we follow the method in [77]. The pressure equation is solved by standard mixed finite element method with RT_0 finite element space and the saturation equation is solved by explicit upwinding finite volume method.

The data is obtained in a coarse square mesh with coarse mesh size $H = \sqrt{2}/10$, while the nudged parameter $\mu = 200$.

Since we do not have access to true (reference) solutions for these problems, we instead use a computed solution. The reference solutions were evolved from a zero initial value, and is run to $t = 325$ using the above setting. For the DA computation, we start from zero initial conditions use the same spatial and temporal discretization parameters as the reference solution, and start assimilation with the reference solution at $t = 25$ (i.e., time 0 for DA corresponds to $t = 25$ for the reference).

5.1. Computational study I. In our first experiment, we consider the relative permeability $k_{r\alpha}$ defined as

$$k_{ro} = (1 - S_w)^2, \quad k_{rw} = (S_w)^2,$$

with the injection and production located at the top-left and bottom-right corner of the domain respectively. We consider the source terms q_t, q_w are defined as

$$q_t(t, x) = \begin{cases} \frac{10}{h^2} & x \in \text{the top-left corner finite grid finite element} \\ -\frac{10}{h^2} & x \in \text{the bottom-right corner finite grid element} \end{cases},$$

and

$$q_w(t, x) = \begin{cases} \frac{10}{h^2} & x \in \text{the top-left corner finite grid finite element} \\ -S(t, w) \frac{10}{h^2} & x \in \text{the bottom-right corner finite grid element} \end{cases}.$$

In this experiment, we carried out three tests. The first one is with data taken on full domain Ω , and the other two tests are carried out with data only taken on one of the following square sub-domains at the top - left corner:

$$\Omega_1 = [0, 50]^2, \quad \Omega_2 = [0, 25]^2.$$

The plots in Figure 1 shows the saturation error in L^2 vs. time, where the observational data are collected from different fractions of the domain. The solution without data assimilation $\mu = 0$ has only negligible drop (in blue) in its residual error. This underscores the significance of a nudged solution synchronizing with the reference solution. Full nudging (in red) indicates synchronization with the reference solution roughly at an exponential rate. We then continue by testing the effect of the size of the sub-domain. Machine precision is reached for data collected over the whole domain. By then, in the case of Ω_1 and Ω_2 , the error is within 10^{-10} and 10^{-5} respectively. Particularly in the case of subdomains Ω_1 and Ω_2 , we see from the snapshot plots in Figures 2, 3, 4, and 5 that the main spatial features over the full domain Ω are nevertheless captured as time evolves.

The convergence of the DA solution with decreasing H is shown in table 1. The convergence of the DA solution to the true solution in time can also be seen in the snapshot plots of the solutions in Figure 6. Here at $t = 0.1$, there is of course a major difference, since the DA simulation starts at $t = 0$. The accuracy of DA is seen to increase by $t = 1$ and further by $t = 10$. Finally by $t = 100$ there is no visual difference between DA and reference solution, which we expect since the L^2 difference between the solutions at $t = 100$ is seen in Figure 1 to be near 10^{-15} . Moreover, the snapshot plots of the true solution starting from zero

(H, μ)	$(1/5, 100)$	$(1/10, 200)$	$(1/20, 400)$
L^2 -error at $T = 10$	0.2499	0.0619	0.0080

 TABLE 1. Error convergence with varying H

initial value (bottom plots in Figure 6) indicate the sensitivity of the solution to the initial conditions.

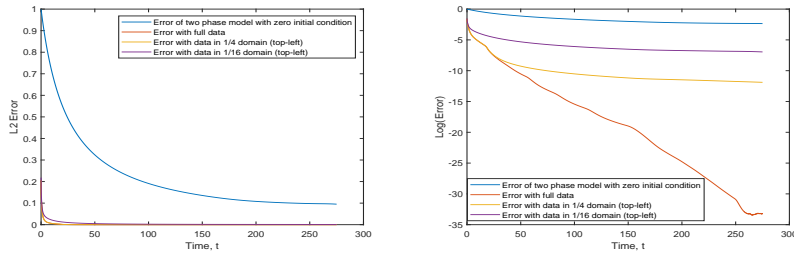


FIGURE 1. Error comparison $\|S(t) - \tilde{S}(t)\|_{L^2}$. Left: L_2 error. Right: L_2 error in log-scale.

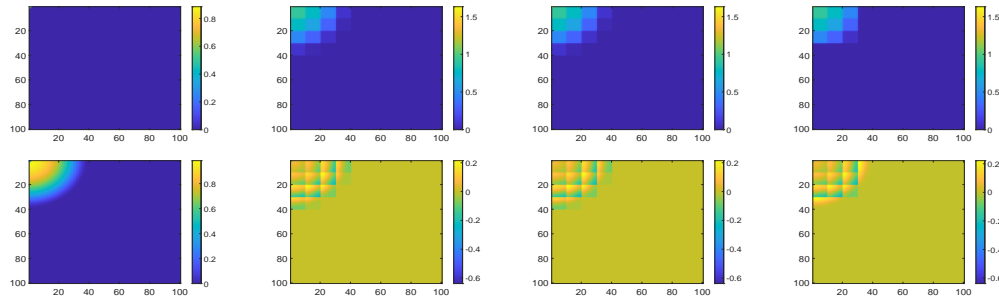


FIGURE 2. Snapshots of S and comparison of the solutions with different data at $T = 0.1$. Top: snapshot of S . Bottom: pointwise error of the solution. Left: two-phase solution. Middle-Left: full data. Middle-Right: $\frac{1}{4}$ data. Right: $\frac{1}{16}$ data

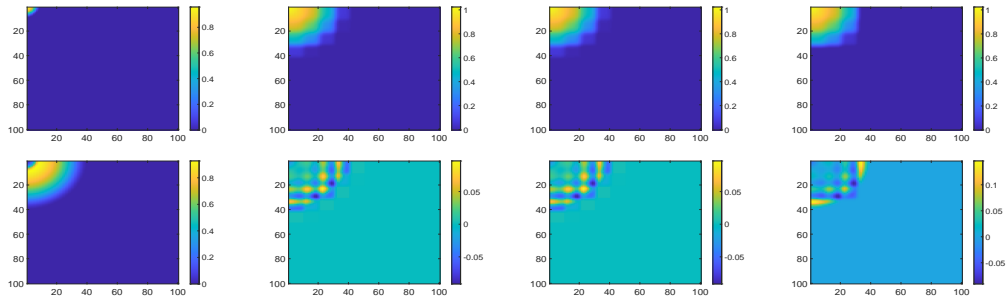


FIGURE 3. Snapshots of S and comparison of the solutions with different data at $T = 1$. Top: snapshot of S . Bottom: pointwise error of the solution. Left: two-phase solution. Middle-Left: full data. Middle-Right: $\frac{1}{4}$ data. Right: $\frac{1}{16}$ data

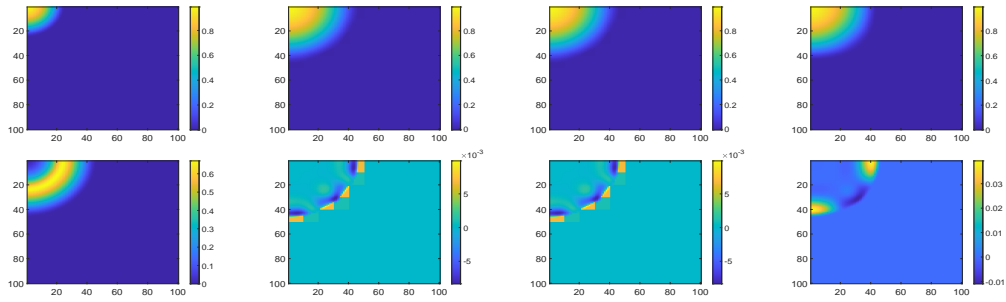


FIGURE 4. Snapshots of S and comparison of the solutions with different data at $T = 10$. Top: snapshot of S . Bottom: pointwise error of the solution. Left: two-phase solution. Middle-Left: full data. Middle-Right: $\frac{1}{4}$ data. Right: $\frac{1}{16}$ data

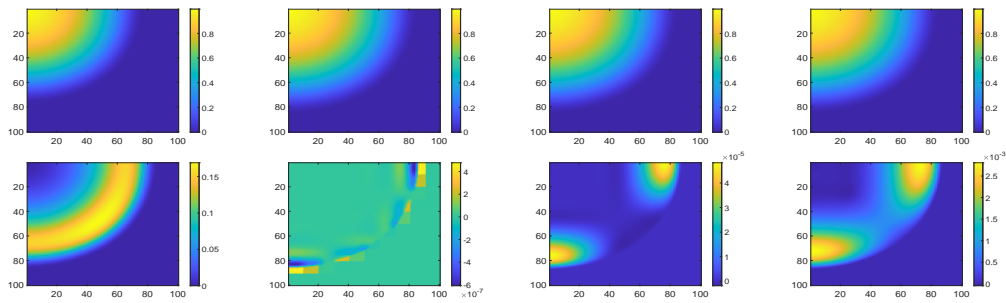


FIGURE 5. Snapshots of S and comparison of the solutions with different data at $T = 100$. Top: snapshot of S . Bottom: pointwise error of the solution. Left: two-phase solution. Middle-Left: full data. Middle-Right: $\frac{1}{4}$ data. Right: $\frac{1}{16}$ data

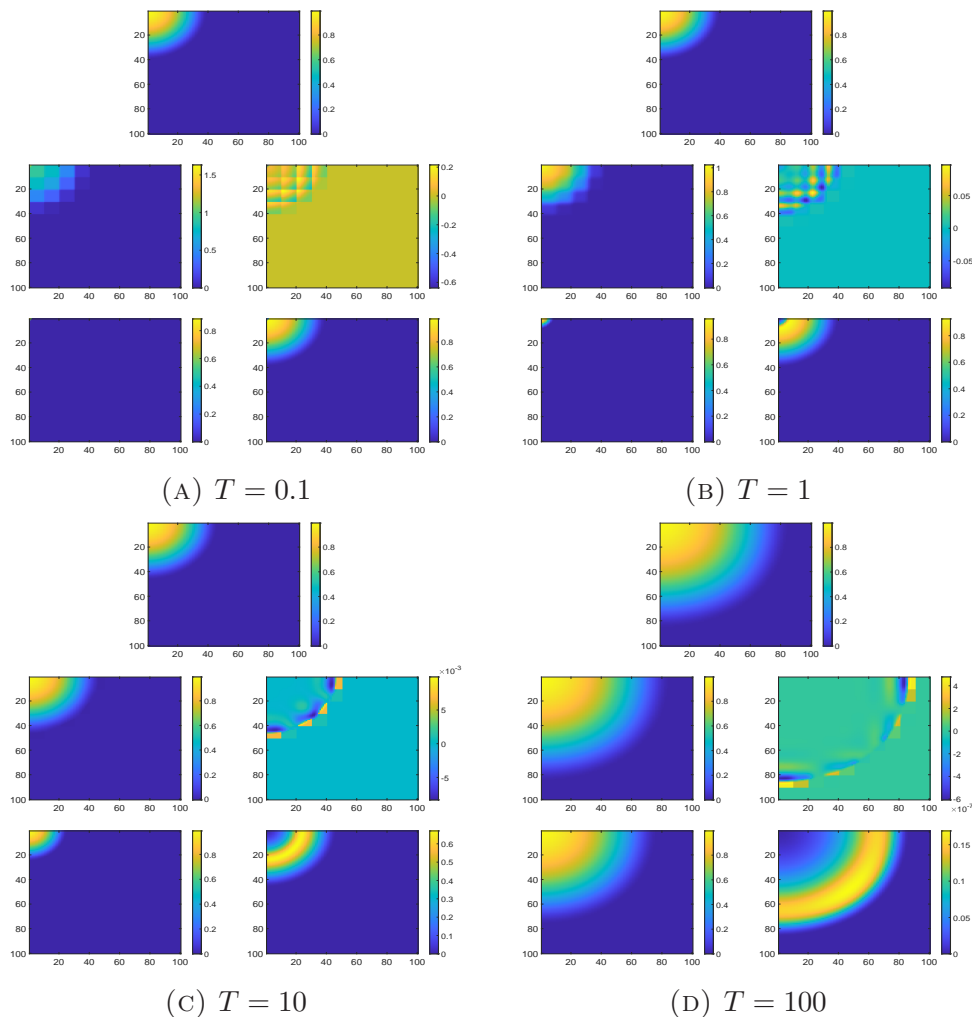


FIGURE 6. Snapshots of the solutions S . Top: Reference solution. Middle-Left: DA (approximate) solution. Middle-Right: difference between the approximate and reference solution. Bottom-Left: two-phase solution starting from zero initial value. Bottom-Right: difference between the two-phase solutions with different initial values.

5.2. Computational study II. We present our second numerical test, with its source terms coinciding with that of the first example. On the other hand, we have a medium that have a totally different permeability profile as shown in figure 7.

The same initialization process as in the first example is considered here, which provides us with the initial condition of the exact solution as $S(0) = \tilde{S}(25)$. With this new medium profile, we compute an approximate solution without any prior knowledge of our initial value, and apply our data assimilation algorithm with $\mu = 200$ as in Example 1. In this experiment, we carried out two tests. The first one is with data taken on full domain Ω , and the other test is carried out with data only taken on one of the following sub-domains at the left half

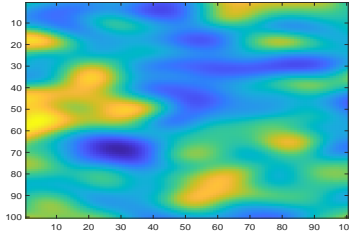


FIGURE 7. Absolute permeability for case 2.

of the domain:

$$\Omega_3 = [0, 50] \times [0, 100].$$

The convergence history of this test is given in Figure 8, and the snapshots of the solutions S are now shown in Figures 13. We again observe an exponential decay of the residual error in Figure 8, with a clear linear fit in the log scale. This has numerically validated the theoretical result that we have proved in Theorem 4.3, and the effectiveness of our proposed data assimilation algorithm. We then continue by testing the effect of the size of the subdomain. In the case of subdomain Ω_3 , we see from the snapshot plots in Figures 9, 10, 11, and 12 that the main spatial features over the full domain Ω are nevertheless captured as time evolves.

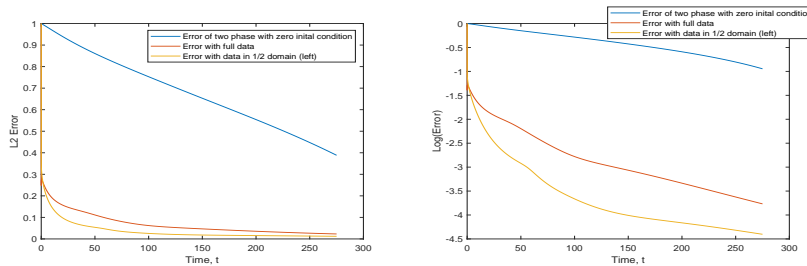


FIGURE 8. Error comparison $\|S(t) - \tilde{S}(t)\|_{L^2}$. Left: L_2 error. Right: L_2 error in log-scale.

6. CONCLUSION

While two-phase models have a long history of success on numerical reservoir simulation, they tend to lose accuracy on more complicated problems due to the insufficient and inaccurate knowledge of the initial state. To overcome this difficulty, the observational measurements can be directly inserted into the mathematical model to improve the accuracy. In our work, we have proposed, analyzed, and tested a novel continuous data assimilation two-phase flow algorithm for reservoir simulation which combines the coarse grid saturation measurement data with the two-phase flow problem. We have shown a stability estimate and an exponentially decaying error bound between the exact and approximate solutions until the error hits a threshold depending on the order of data resolution. We also looked at two numerical computations and observed that synchronization is achievable at a resolution much

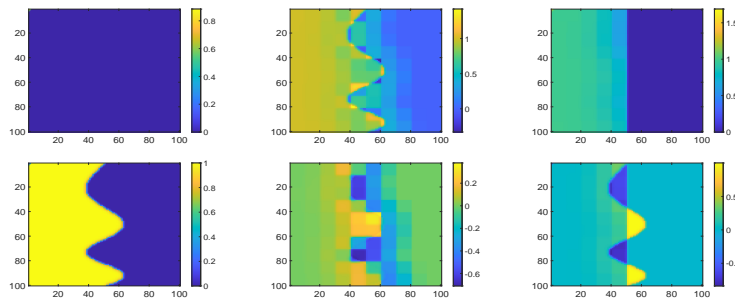


FIGURE 9. Snapshots of S and comparison of the solutions with different data at $T = 0.1$. Top: snapshot of S . Bottom: pointwise error of the solution. Left: two-phase solution. Middle: full data. Right: $\frac{1}{2}$ data

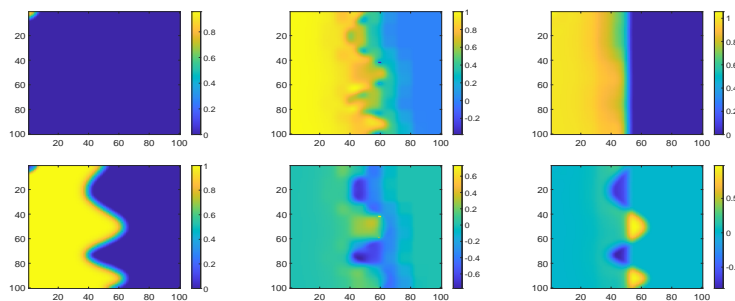


FIGURE 10. Snapshots of S and comparison of the solutions with different data at $T = 1$. Top: snapshot of S . Bottom: pointwise error of the solution. Left: two-phase solution. Middle: full data. Right: $\frac{1}{2}$ data

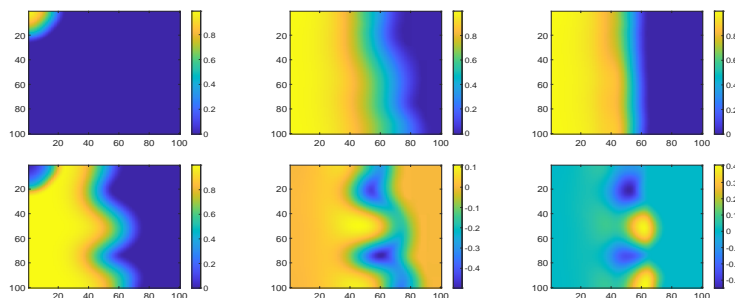


FIGURE 11. Snapshots of S and comparison of the solutions with different data at $T = 10$. Top: snapshot of S . Bottom: pointwise error of the solution. Left: two-phase solution. Middle: full data. Right: $\frac{1}{2}$ data

more coarse than suggested by the rigorous analysis, which is consistent with experiments carried out at other studies. Moreover, we demonstrated numerically that machine precision synchronization is achieved for data collected from a small fraction of the domain. Tests of nudging on moving subdomains are also encouraging, a matter we will explore in a future work.

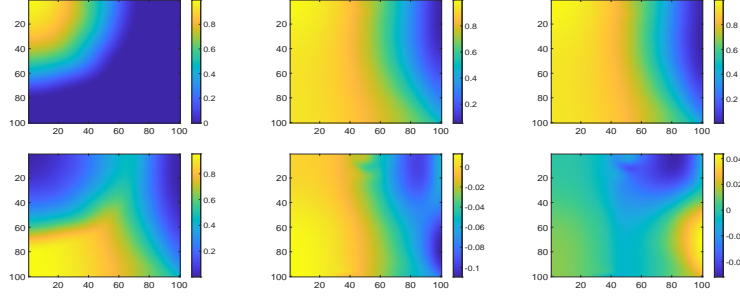


FIGURE 12. Snapshots of S and comparison of the solutions with different data at $T = 100$. Top: snapshot of S . Bottom: pointwise error of the solution. Left: two-phase solution. Middle: full data. Right: $\frac{1}{2}$ data

Future directions include the extension of the method and stability analysis in multi-phase flow and other physically relevant fluid models, e.g. plasma, magneto-fluid, etc, as well as pursuing a stability estimate of our model with partial observation on a small portion of the domain.

Appendices

In this appendix, we prove lemma 3.7, lemma 3.9, lemma 3.10 and theorem 3.11. First, we will present the proof of lemma 3.7.

Proof. Since $P^\eta(t, \cdot) \in V_0$, set $w = P^\eta$ in (3.10) to obtain

$$\begin{aligned} \underline{\kappa}(t_{i+1} - t_i) |P^\eta(t, \cdot)|_K^2 &\leq \int_{t_i}^{t_{i+1}} \int_{\Omega} \kappa(S_w) K |\nabla P^\eta(t, \cdot)|^2 = \int_{t_i}^{t_{i+1}} \int_{\Omega} q_t(t, \cdot) P^\eta(t, \cdot) \\ &\leq C(t_{i+1} - t_i) \|q_t\|_{L^\infty(0, T; H^{-1}(\Omega))} \|P^\eta\|_{L^\infty(0, T; H^1(\Omega))}. \end{aligned}$$

Therefore, we have $c_K \|P^\eta\|_{L^\infty(0, T; V_0)} \leq \|P^\eta\|_{L^\infty(0, T; H^1(\Omega))} \leq C_K \|P^\eta\|_{L^\infty(0, T; V_0)}$ and

$$\|P^\eta\|_{L^\infty(0, T; H^1)} \leq C_K^2 \underline{\kappa}^{-1} \|q_t\|_{L^\infty(0, T; H^{-1}(\Omega))}.$$

Then consider $v = \theta^\eta$ in (3.10) and obtain

$$\int_0^T \int_{\Omega} \left(\partial^\eta(T(\theta^\eta)) \theta^\eta + \kappa_w K \nabla P^\eta \cdot \nabla \theta^\eta + K |\nabla \theta^\eta|^2 \right) = \int_0^T \int_{\Omega} q_w \theta^\eta.$$

After using Lemma 3.6, we have

$$\int_0^T \int_{\Omega} \left(\partial^\eta(T(\theta^\eta)) \theta^\eta \right) \geq - \int_{\Omega} \int_0^{\theta_0} (T(c) - T(\xi)) d\xi,$$

and

$$\int_{\Omega} T(\theta^\eta)(t, \cdot) - \int_{\Omega} T(\theta^\eta)(0, \cdot) = \int_0^t \int_{\Omega} q_w.$$

Hence, we obtain

$$\left| \int_{\Omega} \theta^n(t, \cdot) \right| \leq C \left(\left| \int_{\Omega} \theta^n(0, \cdot) \right| + \left| \int_0^t \int_{\Omega} q_w \right| \right),$$

and therefore

$$\|\theta^n(t, \cdot)\|_{H^1}^2 \leq C \left(\|\theta^n(t, \cdot)\|_{V_0}^2 + \left| \int_0^t \int_{\Omega} q_w \right|^2 + \left| \int_{\Omega} \theta^n(0, \cdot) \right|^2 \right).$$

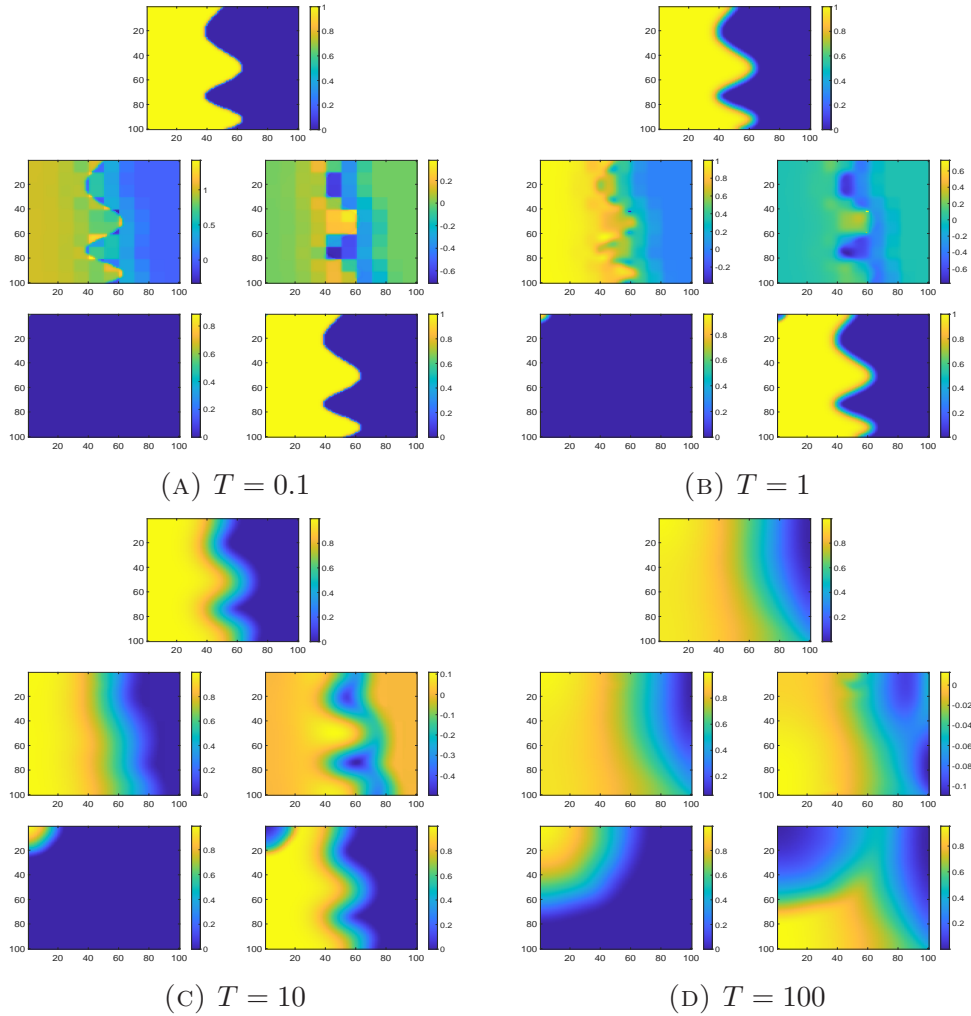


FIGURE 13. Snapshot of the solutions S . Top: Reference solution (exact). Middle-Left: data assimilation solution. Middle-Right: difference between data assimilation solution and reference solution. Bottom-Left: two-phase solution. Bottom-Right: difference between two-phase solution and reference solution.

With the above inequalities, one can arrive at

$$\begin{aligned}
|\theta^\eta|_{L^2(0,T;H^1)}^2 &\leq C |\theta^\eta|_{L^2(0,T;V_0)}^2 + \left| \int_0^t \int_\Omega q_w \right|^2 + \left| \int_\Omega \theta^\eta(0, \cdot) \right|^2 \\
(1) \quad &\leq C \left(\|q_w\|_{L^2(0,T;H^{-1}(\Omega))}^2 + \|q_t\|_{L^2(0,T;H^{-1}(\Omega))}^2 + \int_\Omega \int_0^{\theta_0} (T(\theta_0) - T(\xi)) d\xi \right. \\
&\quad \left. + \left| \int_0^T \int_\Omega |q_w| \right|^2 + \left| \int_\Omega \theta^\eta(0, \cdot) \right|^2 \right).
\end{aligned}$$

□

We will next present the proof of lemma 3.9.

Proof. After subtracting the two equations, we have

$$-\int_0^T \int_\Omega \kappa(S_1) K \nabla(P_2 - P_1) \cdot \nabla w = \int_0^T \int_\Omega (\kappa(S_2) - \kappa(S_1)) K \nabla P_2 \cdot \nabla w + \int_0^T \int_\Omega (q_{t,1} - q_{t,2}) w.$$

for all test function $w \in V_0$. Set $w = P_1 - P_2$ to get

$$\begin{aligned}
(2) \quad &\int_0^T \|\nabla(P_2 - P_1)\|_{L^2}^2 \leq C \int_0^T \int_\Omega \kappa(S_1) K |\nabla(P_2 - P_1)|^2 \\
&= \int_0^T \int_\Omega (\kappa(S_2) - \kappa(S_1)) K \nabla P_2 \cdot \nabla(P_1 - P_2) + \int_0^T \int_\Omega (q_{t,1} - q_{t,2})(P_1 - P_2) \\
&\leq C \int_0^T \|\nabla P_2\|_{L^\infty} \|\kappa(S_2) - \kappa(S_1)\|_{L^2} \|\nabla(P_2 - P_1)\|_{L^2} + \int_0^T \|q_{t,1} - q_{t,2}\|_{L^2} \|P_2 - P_1\|_{L^2}.
\end{aligned}$$

And Since $\|P_2 - P_1\|_{L^2} \leq C \|\nabla(P_2 - P_1)\|_{L^2}$, we obtain the result

$$\|\nabla(P_2 - P_1)\|_{L^2} \leq C (\|\kappa(S_2) - \kappa(S_1)\|_{L^2} + \|q_{t,2} - q_{t,1}\|_{L^2}).$$

□

We then present the proof of lemma 3.10.

Proof. After subtracting the two equations, we get

$$\begin{aligned}
(3) \quad &\int_0^t \int_\Omega \partial_t(S_2 - S_1)v + K \nabla(\theta_2 - \theta_1) \cdot \nabla v + \kappa_w(S_1) K \nabla(P_2 - P_1) \cdot \nabla v \\
&= \int_0^t \int_\Omega (\kappa_w(S_1) - \kappa_w(S_2)) K \nabla P_2 \cdot \nabla v + \int_0^t (q_{w,1} - q_{w,2}, v),
\end{aligned}$$

for all test functions $v \in L^2(0, T; H^1(\Omega))$. Using Definition 2.2, we have the following estimates on the first two terms of the above equations

$$\int_\Omega \partial_t(S_2 - S_1)G(e) = \int_\Omega \partial_t(e)G(e) = a(G(\partial_t(e)), G(e)) = \frac{1}{2} \partial_t \|G(e)\|_{V_0}^2 = \frac{1}{2} \partial_t \|e\|_{V_0^*}^2,$$

and

$$\int_\Omega K \nabla(\theta_2 - \theta_1) \cdot \nabla G(e) = a(\theta_2 - \theta_1, G(e)) = (\theta_2 - \theta_1, e)$$

$$= (\theta_2 - \theta_1, S_2 - S_1) - (\theta_2 - \theta_1, \pi(S_2 - S_1)).$$

By Holder's inequality and Young's inequality, we then obtain

$$\begin{aligned} \int_{\Omega} K \nabla(\theta_2 - \theta_1) \cdot \nabla G(e) &\geq (\theta_2 - \theta_1, S_2 - S_1) - \|\theta_2 - \theta_1\|_{L^p} \|\pi(S_2 - S_1)\|_{L^q} \\ &\geq (\theta_2 - \theta_1, S_2 - S_1) - \frac{\delta_p^p}{p} \|\theta_2 - \theta_1\|_{L^p}^p - \frac{1}{q\delta_p^q} \|\pi(S_2 - S_1)\|_{L^q}^q. \end{aligned}$$

Since $P_2 \in L^\infty(0, T; W^{1,\infty}(\Omega))$, the term $\int_0^t \int_{\Omega} (\kappa_w(S_1) - \kappa_w(S_2)) K \nabla P_2 \cdot \nabla G(e)$ in (3) can be estimated as

$$\begin{aligned} \int_0^t \int_{\Omega} (\kappa_w(S_1) - \kappa_w(S_2)) K \nabla P_2 \cdot \nabla G(e) &\leq C \|P_2\|_{L^\infty(0,T,W^{1,\infty})} \int_0^t \int_{\Omega} |(\kappa_w(S_1) - \kappa_w(S_2))| \cdot |\nabla G(e)| \\ &\leq C \int_0^t \|\kappa_w(S_1) - \kappa_w(S_2)\|_{L^2} \|\nabla G(e)\|_{L^2} \\ &\leq C \int_0^t \left(\frac{\delta}{2} \|\kappa(S_2) - \kappa(S_1)\|_{L^2}^2 + \frac{1}{2\delta} \|\nabla G(e)\|_{L^2}^2 \right). \end{aligned}$$

Similarly, the other two terms $\int_0^t (q_{w,1} - q_{w,2}, G(e))$ and $\int_0^t \int_{\Omega} \kappa_w(S_1) K \nabla(P_2 - P_1) \cdot \nabla G(e)$ in (3) can be bounded above as

$$\int_0^t (q_{w,1} - q_{w,2}, G(e)) \leq \int_0^t \frac{\delta}{2} \|q_{w,1} - q_{w,2}\|_{L^2}^2 + \frac{1}{2\delta} \int_0^t \|G(e)\|_{L^2}^2,$$

and

$$\int_0^t \int_{\Omega} \kappa_w(S_1) K \nabla(P_2 - P_1) \cdot \nabla G(e) \leq C \int_0^t \left(\frac{\delta}{2} \|\nabla(P_2 - P_1)\|_{L^2}^2 + \frac{1}{2\delta} \|\nabla G(e)\|_{L^2}^2 \right).$$

After inserting the above estimates into (3), we obtain

$$\begin{aligned} &\frac{1}{2} \partial_t \int_0^t \|e\|_{V_0^*}^2 + \int_0^t (\theta_2 - \theta_1, S_2 - S_1) \\ &\leq \frac{\delta_p^p}{p} \int_0^t \|\theta_2 - \theta_1\|_{L^p}^p + \frac{1}{q\delta_p^q} \int_0^t \|\pi(S_2 - S_1)\|_{L^q}^q + C \frac{1}{2\delta} \int_0^t (\|\nabla G(e)\|_{L^2}^2 + \|G(e)\|_{L^2}^2) \\ &+ C \frac{\delta}{2} \int_0^t (\|\kappa(S_2) - \kappa(S_1)\|_{L^2}^2 + \|\nabla(P_2 - P_1)\|_{L^2}^2 + \|q_{w,1} - q_{w,2}\|_{L^2}^2), \end{aligned}$$

for some constant $C > 0$. Since $|\theta_2 - \theta_1| \leq C|S_2 - S_1|$ and $\|e\|_{L^2} \leq C\|\nabla G(e)\|_{L^2}$, we have

$$\begin{aligned} &\frac{1}{2} \partial_t \int_0^t \|e\|_{V_0^*}^2 + \int_0^t (\theta_2 - \theta_1, S_2 - S_1) \\ &\leq \frac{\delta_p^p}{p} \int_0^t \|S_2 - S_1\|_{L^p}^p + \frac{1}{q\delta_p^q} \int_0^t \|\pi(S_2 - S_1)\|_{L^q}^q + C \frac{1}{2\delta} \int_0^t \|\nabla G(e)\|_{L^2}^2 \\ &+ C \frac{\delta}{2} \int_0^t (\|\kappa(S_2) - \kappa(S_1)\|_{L^2}^2 + \|\nabla(P_2 - P_1)\|_{L^2}^2 + \|q_{w,1} - q_{w,2}\|_{L^2}^2). \end{aligned}$$

Then consider $v = \pi(S_2 - S_1)$ in (3), and obtain

$$\begin{aligned} \frac{1}{q} \left(\|\pi(S_2 - S_1)(t, \cdot)\|_{L^q}^q - \|\pi(S_2 - S_1)(0, \cdot)\|_{L^q}^q \right) &= \int_0^t \int_{\Omega} \partial_t(S_2 - S_1)(\pi(S_2 - S_1))^{q-1} \\ &= \int_0^t (q_{w,2} - q_{w,1}, (\pi(S_2 - S_1))^{q-1}). \end{aligned}$$

Therefore, we have

$$\frac{1}{q} \|\pi(S_2 - S_1)\|_{L^q(0,t;L^q)}^q \leq \|\pi(S_2 - S_1)\|_{L^q(0,t;L^q)}^{q-1} \|q_{w,2} - q_{w,1}\|_{L^q(0,t;L^q)} + \frac{1}{q} \|\pi(S_2 - S_1)(0, \cdot)\|_{L^q(\Omega)}^q,$$

and

$$\|\pi(S_2 - S_1)\|_{L^q(0,t;L^q)}^q \leq C_q \left(\|\pi(S_2 - S_1)(0, \cdot)\|_{L^q}^q + \|q_{w,2} - q_{w,1}\|_{L^q(0,t;L^q)}^q \right),$$

which proves the lemma. \square

Finally, we will present the proof of theorem 3.11

Proof. From Lemma 3.9, we have

$$\|\nabla(P_2 - P_1)\|_{L^2}^2 \leq C \left(\|\kappa(S_2) - \kappa(S_1)\|_{L^2}^2 + \|q_{t,2} - q_{t,1}\|_{L^2}^2 \right).$$

Therefore, we observe that

$$\begin{aligned} &\frac{1}{2} \partial_t \int_0^t \|e\|_{V_0^*}^2 + \int_0^t (\theta_2 - \theta_1, S_2 - S_1) \\ &\leq \frac{\delta^p}{p} \int_0^t \|S_1 - S_2\|_{L^p}^p + \frac{C_q}{q\delta_p^q} \left(\|\pi(S_2 - S_1)(0, \cdot)\|_{L^q}^q + \|q_{w,2} - q_{w,1}\|_{L^q(0,t;L^q)}^q \right) \\ &\quad + C \frac{\delta}{2} \int_0^t \left(\|\kappa(S_2) - \kappa(S_1)\|_{L^2}^2 + \|q_{w,2} - q_{w,1}\|_{L^2}^2 + \|q_{t,2} - q_{t,1}\|_{L^2}^2 \right) + C \frac{1}{2\delta} \int_0^t \|\nabla G(e)\|_{L^2}^2. \end{aligned}$$

Since $|\kappa(S_2) - \kappa(S_1)| \leq (\theta_2 - \theta_1)(S_2 - S_1)$, we have

$$\begin{aligned} &\frac{1}{2} \partial_t \int_0^t \|e\|_{V_0^*}^2 + \left(1 - \frac{C\delta}{2}\right) \int_0^t (\theta_2 - \theta_1, S_2 - S_1) \\ &\leq \frac{\delta^p}{p} \int_0^t \|S_1 - S_2\|_{L^p}^p + \frac{C_q}{q\delta_p^q} \left(\|\pi(S_2 - S_1)(0, \cdot)\|_{L^q}^q + \|q_{w,2} - q_{w,1}\|_{L^q(0,t;L^q)}^q \right) \\ &\quad + C \frac{\delta}{2} \int_0^t \left(\|q_{w,2} - q_{w,1}\|_{L^2}^2 + \|q_{t,2} - q_{t,1}\|_{L^2}^2 \right) + C \frac{1}{2\delta} \int_0^t \|\nabla G(e)\|_{L^2}^2. \end{aligned}$$

By taking $\delta = C^{-1}$ in the above inequality, we obtain

$$\begin{aligned} &\partial_t \int_0^t \|e\|_{V_0^*}^2 + \int_0^t (\theta_2 - \theta_1, S_2 - S_1) \\ &\leq 2 \left(\frac{\delta^p}{p} \int_0^t \|S_1 - S_2\|_{L^p}^p + \frac{C_q}{q\delta_p^q} \left(\|\pi(S_2 - S_1)(0, \cdot)\|_{L^q}^q + \|q_{w,2} - q_{w,1}\|_{L^q(0,t;L^q)}^q \right) \right) \\ &\quad + \frac{1}{2} \int_0^t \left(\|q_{w,2} - q_{w,1}\|_{L^2}^2 + \|q_{t,2} - q_{t,1}\|_{L^2}^2 \right) + \frac{C^2}{2} \int_0^t \|\nabla G(e)\|_{L^2}^2. \end{aligned}$$

Since $\int_0^t (\theta_2 - \theta_1, S_2 - S_1) \geq C \int_0^t \int_\Omega |S_2 - S_1|^{2+\tau}$, we can choose a $\delta_p > 0$ such that

$$\begin{aligned} & \partial_t \int_0^t \|e\|_{V_0^*}^2 + \frac{1}{2} \int_0^t (\theta_2 - \theta_1, S_2 - S_1) \\ & \leq C \left(\|\pi(S_2 - S_1)(0, \cdot)\|_{L^{q_0}}^{q_0} + \|q_{w,2} - q_{w,1}\|_{L^{q_0}(0,T;L^{q_0})}^{q_0} \right) \\ & + C \int_0^t \|\nabla G(e)\|_{L^2}^2 + \frac{1}{2} \|q_{w,2} - q_{w,1}\|_{L^2(0,T;L^2)}^2 + \frac{1}{2} \|q_{t,2} - q_{t,1}\|_{L^2(0,T;L^2)}^2. \end{aligned}$$

Then denote $E = \|\nabla G(e)\|_{L^2}^2$, and since

$$\|e\|_{V_0^*}^2 = \int_\Omega K |\nabla G(e)|^2 \geq c \|\nabla G(e)\|_{L^2}^2 = c E,$$

and

$$\|\nabla G(e)\|_{L^{q_p}}^{q_p} \leq C \|\nabla G(e)\|_{L^2}^{q_p},$$

we can get

$$\begin{aligned} & E(t) - E(0) + \frac{1}{2} \int_0^t (\theta_2 - \theta_1, S_2 - S_1) \\ & \leq C \int_0^t E + C \left(\|\pi(S_2 - S_1)(0, \cdot)\|_{L^{q_0}(\Omega)}^{q_0} + \|q_{w,2} - q_{w,1}\|_{L^{q_0}(0,T;L^{q_0}(\Omega))}^{q_0} \right) \\ & + \frac{1}{2} \left(\|q_{w,2} - q_{w,1}\|_{L^2(0,T;L^2(\Omega))}^2 + \|q_{t,2} - q_{t,1}\|_{L^2(0,T;L^2(\Omega))}^2 \right). \end{aligned}$$

With that, we at last arrive at

$$\begin{aligned} E(t) \leq C e^{Ct} & \left(\|\pi(S_2 - S_1)(0, \cdot)\|_{L^{q_0}}^{q_0} + \|q_{w,2} - q_{w,1}\|_{L^{q_0}(0,T;L^{q_0})}^{q_0} + E(0) \right. \\ & \left. + \|q_{w,2} - q_{w,1}\|_{L^2(0,T;L^2)}^2 + \|q_{t,2} - q_{t,1}\|_{L^2(0,T;L^2)}^2 \right), \end{aligned}$$

where $q_0 = \frac{2+\tau}{1+\tau}$. □

REFERENCES

- [1] S. Aanonsen, G. Nævdal, D. S. Oliver, A. C. Reynolds, and B. Vallès, *The ensemble Kalman filter in reservoir engineering—a review*, Spe Journal **14** (2009), no. 03, 393–412.
- [2] H. W. Alt and E. Di Benedetto, *Nonsteady flow of water and oil through inhomogeneous porous media*, Annali della Scuola Normale Superiore di Pisa-Classe di Scienze **12** (1985), no. 3, 335–392.
- [3] B. Amaziane, L. Pankratov, and A. Piatnitski, *The existence of weak solutions to immiscible compressible two-phase flow in porous media: the case of fields with different rock-types*, Discrete & Continuous Dynamical Systems-B **18** (2013), no. 5, 1217.
- [4] S. N. Antontsev, A. Kazhikov, and V. N. Monakhov, *Boundary value problems in mechanics of nonhomogeneous fluids*, Elsevier, 1989.
- [5] T. Arbogast, *The existence of weak solutions to single porosity and simple dual-porosity models of two-phase incompressible flow* (1992).
- [6] M. Asch, M. Bocquet, and M. Nodet, *Data assimilation*, Fundamentals of Algorithms, vol. 11, Society for Industrial and Applied Mathematics (SIAM), Philadelphia, PA, 2016. Methods, algorithms, and applications.

- [7] M. U. Altaf, E. S. Titi, T. Gebrael, O. M. Knio, L. Zhao, M. F. McCabe, and I. Hoteit, *Downscaling the 2D Bénard convection equations using continuous data assimilation*, *Comput. Geosci.* **21** (2017), no. 3, 393–410.
- [8] M. Asch, M. Bocquet, and M. Nodet, *Data assimilation*, *Fundamentals of Algorithms*, vol. 11, Society for Industrial and Applied Mathematics (SIAM), Philadelphia, PA, 2016. Methods, algorithms, and applications.
- [9] D. Auroux and J. Blum, *A nudging-based data assimilation method: the Back and Forth Nudging (BFN) algorithm*, *Nonlin. Processes Geophys.* **15** (2008), 305–319.
- [10] A. Azouani, E. Olson, and E. S. Titi, *Continuous data assimilation using general interpolant observables*, *J. Nonlinear Sci.* **24** (2014), no. 2, 277–304.
- [11] ———, *Feedback control of nonlinear dissipative systems by finite determining parameter – a reaction-diffusion paradigm*, *Evol. Equ. Control Theory* **3** (2014), no. 4, 579–594.
- [12] H. Bessaih, E. Olson, and E. S. Titi, *Continuous data assimilation with stochastically noisy data*, *Nonlinearity* **28** (2015), no. 3, 729–753.
- [13] A. Biswas, K. Brown, and V. Martinez, *Higher-order synchronization for a data assimilation algorithm with nodal value observables for the Navier-Stokes equation*, preprint (2021).
- [14] A. Biswas, C. Foias, C. F. Mondaini, and E. S. Titi, *Downscaling data assimilation algorithm with applications to statistical solutions of the Navier-Stokes equations*, *Ann. Inst. H. Poincaré Anal. Non Linéaire* **36** (2019), no. 2, 295–326.
- [15] A. Biswas, J. Hudson, A. Larios, and Y. Pei, *Continuous data assimilation for the 2D magnetohydrodynamic equations using one component of the velocity and magnetic fields*, *Asymptot. Anal.* **108** (2018), no. 1-2, 1–43.
- [16] A. Biswas, M. Jolly, and Z. Bradshaw, *Data assimilation for the Navier-Stokes equations using local observables*, *SIAM J. Appl. Dyn. Sys.* (**to appear**) (2021).
- [17] A. Biswas, K. R. Brown, and V. R. Martinez, *Higher-order synchronization of a nudging-based algorithm for data assimilation for the 2D NSE: a refined paradigm for global interpolant observables*, arXiv:2108.05309 (2021).
- [18] M. Blunt, M. J. King, and H. Scher, *Simulation and theory of two-phase flow in porous media*, *Physical review A* **46** (1992), no. 12, 7680.
- [19] C. Cancès and M. Pierre, *An existence result for multidimensional immiscible two-phase flows with discontinuous capillary pressure field*, *SIAM Journal on Mathematical Analysis* **44** (2012), no. 2, 966–992.
- [20] Y. Cao, M. S. Jolly, E. S. Titi, and J. P. Whitehead, *Algebraic bounds on the Rayleigh-Bénard attractor*, *Nonlinearity* **34** (2021), no. 1, 509–531.
- [21] Y. Cao, A. Giorgini, M. Jolly, and A. Pakzad, *Continuous data assimilation for the 3D Ladyzhenskaya model: analysis and computations*, submitted, arXiv:2108.03513 (2021).
- [22] J. Charney, M. Halem, and R. Jastrow, *Use of incomplete historical data to infer the present state of the atmosphere*, *J. Atmos. Sci.* **26** (1969), 1160–1163.
- [23] G. Chavent and J. Jaffré, *Mathematical models and finite elements for reservoir simulation: single phase, multiphase and multicomponent flows through porous media*, Elsevier, 1986.
- [24] Z. Chen, *Degenerate two-phase incompressible flow: I. existence, uniqueness and regularity of a weak solution*, *Journal of Differential Equations* **171** (2001), no. 2, 203–232.
- [25] ———, *Degenerate two-phase incompressible flow II: Regularity, stability and stabilization*, *Journal of Differential Equations* **186** (2002), no. 2, 345–376.
- [26] Z. Chen and R. E. Ewing, *From single-phase to compositional flow: applicability of mixed finite elements*, *Transport in Porous Media* **27** (1997), no. 2, 225–242.
- [27] B. Cockburn, D. A. Jones, and E. S. Titi, *Estimating the number of asymptotic degrees of freedom for nonlinear dissipative systems*, *Math. Comp.* **66** (1997), no. 219, 1073–1087.
- [28] P. Constantin and C. Foias, *Navier-Stokes equations*, *Chicago Lectures in Mathematics*, University of Chicago Press, Chicago, IL, 1988.
- [29] P. Constantin, C. Foias, O. P. Manley, and R. Temam, *Determining modes and fractal dimension of turbulent flows*, *J. Fluid Mech.* **150** (1985), 427–440.

- [30] J. A. De Loera, J. Rambau, and F. Santos, *Triangulations, Algorithms and Computation in Mathematics*, vol. 25, Springer-Verlag, Berlin, 2010. Structures for algorithms and applications.
- [31] G. Evensen, *Data assimilation*, Second, Springer-Verlag, Berlin, 2009. The ensemble Kalman filter.
- [32] A. Farhat, N. E. Glatt-Holtz, V. R. Martinez, S. A. McQuarrie, and J. P. Whitehead, *Data assimilation in large Prandtl Rayleigh-Bénard convection from thermal measurements*, SIAM J. Appl. Dyn. Syst. **19** (2020), no. 1, 510–540.
- [33] A. Farhat, H. Johnston, M. Jolly, and E. S. Titi, *Assimilation of nearly turbulent Rayleigh-Bénard flow through vorticity or local circulation measurements: a computational study*, J. Sci. Comput. **77** (2018), no. 3, 1519–1533.
- [34] A. Farhat, M. Jolly, and E. S. Titi, *Continuous data assimilation for the 2D Bénard convection through velocity measurements alone*, Phys. D **303** (2015), 59–66.
- [35] A. Farhat, E. Lunasin, and E. S. Titi, *A data assimilation algorithm: the paradigm of the 3D Leray- α model of turbulence*, Partial differential equations arising from physics and geometry, London Math. Soc. Lecture Note Ser., vol. 450, Cambridge Univ. Press, Cambridge, 2019, pp. 253–273.
- [36] ———, *Continuous data assimilation for a 2D Bénard convection system through horizontal velocity measurements alone*, J. Nonlinear Sci. **27** (2017), no. 3, 1065–1087.
- [37] ———, *Data assimilation algorithm for 3D Bénard convection in porous media employing only temperature measurements*, J. Math. Anal. Appl. **438** (2016), no. 1, 492–506.
- [38] ———, *Abridged continuous data assimilation for the 2D Navier-Stokes equations utilizing measurements of only one component of the velocity field*, J. Math. Fluid Mech. **18** (2016), no. 1, 1–23.
- [39] A. Farhat, M. Jolly, and E. S. Titi, *Continuous data assimilation for the 2D Bénard convection through velocity measurements alone*, Phys. D **303** (2015), 59–66.
- [40] A. Farhat, E. Lunasin, and E. S. Titi, *Abridged continuous data assimilation for the 2D Navier-Stokes equations utilizing measurements of only one component of the velocity field*, J. Math. Fluid Mech. **18** (2016), no. 1, 1–23.
- [41] C. Foias, C. F. Mondaini, and E. S. Titi, *A discrete data assimilation scheme for the solutions of the two-dimensional Navier-Stokes equations and their statistics*, SIAM J. Appl. Dyn. Syst. **15** (2016), no. 4, 2109–2142.
- [42] C. Foias and G. Prodi, *Sur le comportement global des solutions non-stationnaires des équations de Navier-Stokes en dimension 2*, Rend. Sem. Mat. Univ. Padova **39** (1967), 1–34.
- [43] B. García-Archilla, J. Novo, and E. S. Titi, *Uniform in time error estimates for a finite element method applied to a downscaling data assimilation algorithm for the Navier-Stokes equations*, SIAM J. Numer. Anal. **58** (2020), no. 1, 410–429.
- [44] M. Gesho, E. Olson, and E. S. Titi, *A computational study of a data assimilation algorithm for the two-dimensional Navier-Stokes equations*, Commun. Comput. Phys. **19** (2016), no. 4, 1094–1110.
- [45] W. D. Henshaw, H. Kreiss, and J. Yström, *Numerical experiments on the interaction between the large- and small-scale motions of the Navier-Stokes equations*, Multiscale Model. Simul. **1** (2003), no. 1, 119–149.
- [46] J. Hudson and M. Jolly, *Numerical efficacy study of data assimilation for the 2D magnetohydrodynamic equations*, J. Comput. Dyn. **6** (2019), no. 1, 131–145.
- [47] J. E. Hoke and R. A. Anthes, *The initialization of numerical models by a dynamic initialization technique*, Monthly Weather Review **104** (1976), 1551–1556.
- [48] H. A. Ibdah, C. F. Mondaini, and E. S. Titi, *Fully discrete numerical schemes of a data assimilation algorithm: uniform-in-time error estimates*, IMA J. Numer. Anal. **40** (2020), no. 4, 2584–2625.
- [49] M. S. Jolly, V. R. Martinez, E. J. Olson, and E. S. Titi, *Continuous data assimilation with blurred-in-time measurements of the surface quasi-geostrophic equation*, Chin. Ann. Math. Ser. B **40** (2019), no. 5, 721–764.
- [50] M. Jolly and A. Pakzad, *Data assimilation with higher order finite element interpolants*, submitted [arXiv:2108.03631](https://arxiv.org/abs/2108.03631) (2021).
- [51] M. Jolly, T. Sadigov, and E. S. Titi, *Determining form and data assimilation algorithm for weakly damped and driven Korteweg-de Vries equation—Fourier modes case*, Nonlinear Anal. Real World Appl. **36** (2017), 287–317.

- [52] M. Jolly, V. R. Martinez, and E. S. Titi, *A data assimilation algorithm for the subcritical surface quasi-geostrophic equation*, Adv. Nonlinear Stud. **17** (2017), no. 1, 167–192.
- [53] D. A. Jones and E. S. Titi, *Determining finite volume elements for the 2D Navier-Stokes equations*, Phys. D **60** (1992), no. 1-4, 165–174. Experimental mathematics: computational issues in nonlinear science (Los Alamos, NM, 1991).
- [54] D. A. Jones and E. S. Titi, *Upper bounds on the number of determining modes, nodes, and volume elements for the Navier-Stokes equations*, Indiana Univ. Math. J. **42** (1993), no. 3, 875–887.
- [55] L. Jiang and N. Ou, *Multiscale model reduction method for Bayesian inverse problems of subsurface flow*, Journal of Computational and Applied Mathematics **319** (2017), 188–209.
- [56] E. J. Kostelich, Y. Kuang, J. M. McDaniel, N. Z. Moore, N. L. Martirosyan, and M. C. Preul, *Accurate state estimation from uncertain data and models: an application of data assimilation to mathematical models of human brain tumors*, Biology direct **6** (2011), no. 1, 1–20.
- [57] B. H. Kueper and E. O. Frind, *Two-phase flow in heterogeneous porous media: 1. Model development*, Water Resources Research **27** (1991), no. 6, 1049–1057.
- [58] J. McDaniel, E. Kostelich, Y. Kuang, J. Nagy, M. C. Preul, N. Z. Moore, and N. L. Matirosyan, *Data assimilation in brain tumor models*, Lect. Notes Math. Model. Life Sci., Springer, New York, 2013.
- [59] A. Larios, L. Rebholz, and C. Zervas, *Global in time stability and accuracy of IMEX-FEM data assimilation schemes for Navier-Stokes equations*, Comput. Methods Appl. Mech. Engrg. **345** (2019), 1077–1093.
- [60] K. Law, A. Stuart, and K. Zygalakis, *Data assimilation*, Texts in Applied Mathematics, vol. 62, Springer, Cham, 2015. A mathematical introduction.
- [61] E. Lunasin and E. S. Titi, *Finite determining parameters feedback control for distributed nonlinear dissipative systems—a computational study.*, Evol. Equ. Control Theory, **6** (2017), 535–557.
- [62] C. F. Mondaini and E. S. Titi, *Uniform-in-time error estimates for the postprocessing Galerkin method applied to a data assimilation algorithm*, SIAM J. Numer. Anal. **56** (2018), no. 1, 78–110.
- [63] E. Kalnay, *Atmospheric modeling, data assimilation, and predictability*, Cambridge Univ Pr, 2003.
- [64] P. A. Markowich, E. S. Titi, and S. Trabelsi, *Continuous data assimilation for the three-dimensional Brinkman-Forchheimer-extended Darcy model*, Nonlinearity **29** (2016), no. 4, 1292–1328.
- [65] D. S. Oliver, A. C. Reynolds, and N. Liu, *Inverse theory for petroleum reservoir characterization and history matching*, 2008.
- [66] K. Osypov, Y. Yang, A. Fournier, N. Ivanova, R. Bachrach, C. E. Yarman, Y. You, D. Nichols, and M. Woodward, *Model-uncertainty quantification in seismic tomography: method and applications*, Geophysical Prospecting **61** (2013), no. 6-Challenges of Seismic Imaging and Inversion Devoted to Goldin, 1114–1134.
- [67] H. Park, C. Scheidt, D. Fenwick, A. Boucher, and J. Caers, *History matching and uncertainty quantification of facies models with multiple geological interpretations*, Computational Geosciences **17** (2013), no. 4, 609–621.
- [68] S. Pawar, S. E. Ahmed, O. San, A. Rasheed, and I. M. Navon, *Long short-term memory embedded nudging schemes for nonlinear data assimilation of geophysical flows*, Physics of Fluids **32** (2020).
- [69] L. M. Pecora and T. L. Carroll, *Synchronization of chaotic systems*, Chaos **25** (2015), no. 9, 097611, 12.
- [70] Y. Pei, *Continuous data assimilation for the 3D primitive equations of the ocean*, Commun. Pure Appl. Anal. **18** (2019), no. 2, 643–661.
- [71] R. Tavakoli, H. Yoon, M. Delshad, A. H. ElSheikh, M. F. Wheeler, and B. W. Arnold, *Comparison of ensemble filtering algorithms and null-space Monte Carlo for parameter estimation and uncertainty quantification using CO₂ sequestration data*, Water Resources Research **49** (2013), no. 12, 8108–8127.
- [72] J. A. Trangenstein and J. B. Bell, *Mathematical structure of the black-oil model for petroleum reservoir simulation*, SIAM Journal on Applied Mathematics **49** (1989), no. 3, 749–783.
- [73] P.A. Vidard, F.-X. Le Dimet, and A. Piacentini, *Determination of optimal nudging coefficients*, Tellus A: Dynamic Meteorology and Oceanography **55** (2003), no. 1, 1-15.
- [74] S. Whitaker, *Flow in porous media II: The governing equations for immiscible, two-phase flow*, Transport in porous media **1** (1986), no. 2, 105–125.
- [75] L. Yeh, *Hölder continuity for two-phase flows in porous media*, Mathematical methods in the applied sciences **29** (2006), no. 11, 1261–1289.

- [76] C. Zervas, L. G. Rebholz, M. Schneier, and T. Iliescu, *Continuous data assimilation reduced order models of fluid flow*, *Comput. Methods Appl. Mech. Engrg.* **357** (2019), 112596, 18.
- [77] R and Helmig Huber R, *Multiphase flow in heterogeneous porous media: A classical finite element method versus an implicit pressure–explicit saturation-based mixed finite element–finite volume approach*, *International Journal for Numerical Methods in Fluids* **29** (1999), no. 8, 899–920.

DEPARTMENT OF MATHEMATICS, UNIVERSITY OF CALIFORNIA, RIVERSIDE, CA, USA
Email address: `yattinc@ucr.edu`

DEPARTMENT OF MATHEMATICS, UNIVERSITY OF CALIFORNIA, IRVINE, CA, USA
Email address: `wtleung@uci.edu`

DEPARTMENT OF MATHEMATICS, INDIANA UNIVERSITY BLOOMINGTON, IN, USA
Email address: `apakzad@iu.edu`